International Journal of Hydrogen Energy 70 (2024) 118–135

Contents lists available at ScienceDirect

International Journal of Hydrogen Energy

journal homepage: www.elsevier.com/locate/he

Thermodynamic (p, ρ, T) characterization of a reference high-calorific natural gas mixture when hydrogen is added up to 20 % (mol/mol)

Daniel Lozano-Martín [a], Fatemeh Pazoki [b], Heinrich Kipphardt [c], Peyman Khanipour [c], Dirk Tuma [c], Alfonso Horrillo [b,d], César R. Chamorro [b,*]

[a] GETEF, Departamento de Física Aplicada, Facultad de Ciencias, Universidad de Valladolid, Paseo de Belén, 7, E-47011, Valladolid, Spain
[b] MYER, Departamento de Ingeniería Energética y Fluidomecánica, Universidad de Valladolid, Paseo del Cauce, 59, E-47011, Valladolid, Spain
[c] BAM Bundesanstalt für Materialforschung und -prüfung, Richard-Willstätter-Str., 11, D-12489, Berlin, Germany
[d] CIDAUT Fundación, Plaza Vicente Aleixandre Campos, 2, E-47151, Boecillo, Valladolid, Spain

ARTICLE INFO

Handling Editor: Søren Juhl Andreasen

Keywords:
Hydrogen-enriched natural gas
Gravimetric preparation
Single-sinker densimeter
High-pressure density
Isothermal compressibility
Reference equations of state

ABSTRACT

The injection of hydrogen into the natural-gas grid is an alternative during the process of a gradual decarbonization of the heat and power supply. When dealing with hydrogen-enriched natural gas mixtures, the performance of the reference equations of state habitually used for natural gas should be validated by using high-precision experimental thermophysical data from multicomponent reference mixtures prepared with the lowest possible uncertainty in composition. In this work, we present experimental density data for an 11-compound high-calorific (hydrogen-free) natural gas mixture and for two derived hydrogen-enriched natural gas mixtures prepared by adding (10 and 20) mol-% of hydrogen to the original standard natural gas mixture. The three mixtures were prepared gravimetrically according to ISO 6142–1 for maximum precision in their composition and thus qualify for reference materials. A single-sinker densimeter was used to determine the density of the mixtures from (250–350) K and up to 20 MPa. The experimental density results of this work have been compared to the densities calculated by three different reference equations of state for natural gas related mixtures: the AGA8-DC92 EoS, the GERG-2008 EoS, and an improved version of the GERG-2008 EoS. While relative deviations of the experimental density data for the hydrogen-free natural gas mixture are always within the claimed uncertainty of the three considered equations of state, larger deviations can be observed for the hydrogen-enriched natural gas mixtures from any of the three equations of state, especially for the lowest temperature and the highest pressures.

1. Introduction

Hydrogen-enriched natural gas, H2NG or HENG, is a mixture of natural gas and hydrogen that can be used on existing natural gas infrastructures with little or even no modification to be applied in advance. The substitution, or at least blending of natural gas with hydrogen, biomethane and synthetic methane (or e-methane), is considered a sustainable technology for a gradual decarbonization of the heat and power supply, with increasing blending fractions planned for these renewable gases with natural gas [1]. In principle, hydrogen can be mixed with natural gas in any ratio, but H2NG mixtures with up to 20 vol-% of H_2 represent the most realistic near-term option due to technical and economic reasons [2–5].

Several issues will need to be addressed before large-scale hydrogen injection into the natural gas grid is achieved [6]. From the point of view of end-use appliances, changes in the combustion properties of the mixture, reflected in its heating value and Wobbe index, can modify the performance of the equipment [7–10]. Another important issue is hydrogen embrittlement, which can affect the mechanical properties of iron and steel pipes [11–13]. Last but not least, the addition of hydrogen to natural gas alters the thermodynamic properties of the mixture, which affects its transport and storage characteristics. The design of the processes involved in the production, transportation, and storage of natural gas and H2NG mixtures, with special mention being given to the custody transfer applications, rely on the accuracy of the volumetric and calorific thermophysical properties obtained from the reference thermodynamic models and equations of state [14,15]. Reference equations of state have also been used to develop alternative methods for estimating the

* Corresponding author.
E-mail address: cesar.chamorro@uva.es (C.R. Chamorro).

https://doi.org/10.1016/j.ijhydene.2024.05.028
Received 2 January 2024; Received in revised form 25 April 2024; Accepted 3 May 2024
Available online 17 May 2024

Table 1
Purity, supplier, molar mass, and critical parameters for the constituting components of the reference natural gas mixtures studied in this work.

Component (CAS no.)	Purity/ mol-%	Supplier	M/ g·mol^{-1}	Critical parameters[a]	
				T_c/K	p_c/ MPa
Methane (74-82-8)	≥99.9995	Linde[b]	16.0428	190.56	4.5992
Hydrogen (1333-74-0)	≥99.9999	Linde[b]	2.01588	33.145	1.2964
Nitrogen (7727-37-9)	≥99.9999	Linde[b]	28.0135	126.19	3.3958
Carbon dioxide (124-38-9)	≥99.9995	Air Liquide[c]	44.0098	304.13	7.3773
Ethane (74-84-0)	≥99.999	Matheson Tri-Gas[d]	30.069	305.32	4.8722
Propane (74-98-6)	≥99.999	Air Liquide[c]	44.0956	369.89	4.2512
n-Butane (106-97-8)	≥99.98	Scott[e]	58.1222	425.13	3.796
Isobutane (75-28-5)	≥99.99	Scott[f]	58.1222	407.81	3.629
n-Pentane (109-66-0)	≥99.8	Sigma-Aldrich[g]	72.1488	469.70	3.3675
Isopentane (78-78-4)	≥99.7	Sigma-Aldrich[g]	72.1488	460.35	3.378
Neopentane (463-82-1)	≥99.0	Linde[b]	72.1488	433.74	3.196
n-Hexane (110-54-3)	≥99.7	Sigma-Aldrich[g]	86.1754	507.82	3.0441

[a] Critical parameters were obtained by using the default equation of state for each substance in REFPROP 10 software [29,30].
[b] Linde AG, Unterschleißheim, Germany.
[c] Air Liquide AG, Düsseldorf, Germany.
[d] Matheson Tri-Gas, Inc., Montgomeryville PA, USA.
[e] Scott UK, Newcastle-under-Lyme, UK.
[f] Scott Specialty Gases, Inc., Plumsteadville PA, USA.
[g] Sigma-Aldrich Chemie GmbH, Steinheim, Germany.

thermophysical properties of natural gas related mixtures without the need for costly on-line measurements of mixture composition [16–18].

Two of the most commonly used reference equations of state for natural-gas related mixtures are the AGA8-DC92 EoS [19], developed by the *American Gas Association (AGA)*, and the GERG-2008 EoS [20,21], from the *Groupe Européen de Recherches Gazières (GERG)*, that are both explicit in the Helmholtz energy. The accuracy of these reference equations of state directly depends on both the accuracy and range of the experimental data from where they were derived. Experimental thermophysical data for the pure components of natural gas and for all corresponding binary mixtures are fundamental for the development and any further improvement of the existing reference equations of state for natural gas [22], while experimental data of reference-quality multicomponent mixtures, resembling the composition of an actual natural gas mixture, are relevant to test their performance at pipeline conditions. Consequently, high-precision experimental thermophysical data originating from reference-quality multicomponent H2NG mixtures, which are prepared with the lowest possible uncertainty in composition, are suitable to test the overall performance of the reference equations of state used for natural gas [23,24].

In this work, we present experimental density measurements for a standard 11-compound high-calorific (H_2-free) natural gas mixture and for two derived H2NG mixtures, obtained by adding 10 % and 20 % (mol/mol) hydrogen to the initial standard natural gas mixture. All mixtures investigated were prepared gravimetrically according to ISO 6142–1 [25] for reference quality and maximum precision in their composition. The density measurements were performed with a high-precision single-sinker densimeter over a temperature range from (250–350) K and up to a maximum pressure of 20 MPa. The experimental density results of this work are compared with the abovementioned three different reference equations of state for natural-gas related mixtures: the AGA8-DC92 EoS, the GERG-2008 EoS, and an improved version of the GERG EoS, which we label as "improved-GERG-2008 EoS" in this study. Experimental density measurements for multicomponent mixtures are scarce and necessary to test the performance of reference EoS.

2. Experimental

2.1. Mixture preparation

Three synthetic natural gas mixtures, designated as G 431 (H_2-free natural gas mixture, BAM cylinder no. 2030–200928), G 453 (H_2-enriched natural gas mixture, G 431 + 10 % H_2, 2036–201115), and G 454 (H_2-enriched natural gas mixture, G 431 + 20 % H_2, 2043–201124), were prepared at the Federal Institute for Materials Research and Testing (BAM Bundesanstalt für Materialforschung und -prüfung, Berlin, Germany). The first mixture, G 431, is an 11-compound mixture representative of a high-calorific natural gas composed mainly of methane (>97 %). The following two mixtures, G 453 and G 454, are made by dilution of hydrogen into the first one until a nominal composition of (10 and 20) mol-%, respectively, is reached. All gas mixtures were prepared in aluminum cylinders of $V = 10$ dm^3 by the gravimetric procedure, according to the standard ISO 6142–1 [25], which yields the lowest uncertainty in the composition, using the pure components of purity and supplier listed in Table 1. These pure components were used without further purification to make several premixtures and dilutions in consecutive filling steps (for a detailed filling scheme see the Supplementary File), determining the mass of the gas constituents using an electronic comparator balance (Sartorius LA 34000P-0CE, Sartorius AG) and a high-precision mechanical balance (Voland HCE 25, Voland Corp.). For each mixture of the nominal target composition (i.e., G 431, G 453, and G 454), two calibration mixtures were prepared independently, so that no correlation between the sample mixture and the calibration mixtures exists. All gas mixtures were homogenized by rolling and heating after finishing gravimetric preparation, with the compositions in molar percentage, x_i, and corresponding expanded ($k = 2$) uncertainties in absolute terms, $U(x_i)$, given in Table 2.

Subsequent to homogenization and prior to shipment to the University of Valladolid (UVa), the composition of each mixture to be investigated was validated by Gas Chromatography (GC) at BAM on a multichannel process analyzer (Siemens MAXUM II, Siemens AG) using the corresponding calibration gases following the procedure (so-called "bracketing") described in the standard ISO 12963 [26]. Additional details of this validation procedure are given in a previously published paper [27]. The results of the analysis are reported in Table S2 of the supplementary material, together with the composition of the corresponding validation mixtures used for this purpose. The uncertainties in the concentration values of each component for the studied mixtures and the corresponding validation mixtures have been calculated using the law of propagation of uncertainty and the procedure specified in the Guide to the Expression of Uncertainty in Measurement (GUM) [28], from the purity of the constituents of the mixture, considering the mixture preparation procedure explained in detail in the Supplementary Material. The deviations between gravimetric composition and that from GC analysis had to be sufficiently low as to pass the criteria for certification established by BAM.

The molar mass M, normalized density ρ_n, higher heating value HHV, and Wobbe index W_s for the three mixtures, estimated with the REFPROP 10 software [29,30] from the normalized composition and at reference conditions of 288.15 K and 0.101325 MPa, are also included in Table 2. It can be seen from these values that the G 431 mixture is a typical high-calorific natural gas mixture and that the addition of hydrogen results in a decrease in the normalized density, the higher heating value and the Wobbe index. The higher heating value per unit of volume of the H_2-enriched natural gas mixtures decreases by 7 % and 14

Table 2
Composition of the reference natural gas mixtures studied in this work. Impurity compounds are marked in *italic* type.

Component	G 431 BAM no: 2030–200928		G 453 (G 431 + 10 % H_2) BAM no: 2036–201115		G 454 (G 431 + 20 % H_2) BAM no: 2043–201124	
	$10^2\ x_i$/(mol/mol)	$10^2\ U(x_i)$/(mol/mol)	$10^2\ x_i$/(mol/mol)	$10^2\ U(x_i)$/(mol/mol)	$10^2\ x_i$/(mol/mol)	$10^2\ U(x_i)$/(mol/mol)
Methane	97.2361	0.0020	87.5221	0.0023	77.7981	0.0023
Hydrogen	–	–	9.9928	0.0031	19.9945	0.0046
Nitrogen	1.40097	0.00028	1.25838	0.00024	1.11842	0.00027
Carbon dioxide	0.361460	0.000113	0.324953	0.000092	0.288529	0.000084
Ethane	0.398705	0.000033	0.360839	0.000031	0.320307	0.000031
Propane	0.201221	0.000020	0.180328	0.000019	0.160279	0.000019
n-Butane	0.100398	0.000052	0.090235	0.000047	0.079774	0.000042
Isobutane	0.100431	0.000023	0.090531	0.000021	0.079823	0.000019
n-Pentane	0.050072	0.000023	0.045181	0.000021	0.040107	0.000019
Isopentane	0.049928	0.000023	0.045043	0.000021	0.040017	0.000019
Neopentane	0.050781	0.000022	0.044754	0.000020	0.039945	0.000018
n-Hexane	0.049883	0.000018	0.044883	0.000016	0.040092	0.000015
Oxygen	*0.000012*	*0.000012*	*0.000014*	*0.000010*	*0.000014*	*0.000011*
Hydrogen	*0.000003*	*0.000003*	–	–	–	–
Carbon monoxide	*0.0000003*	*0.0000003*	*0.000001*	*0.000001*	*0.000002*	*0.000002*
Propene	*0.0000002*	*0.0000002*	*0.0000002*	*0.0000002*	*0.0000002*	*0.0000002*
Ethene	*0.00000004*	*0.00000005*	*0.00000004*	*0.00000004*	*0.00000003*	*0.00000004*
Nitric oxide	*0.00000002*	*0.00000002*	*0.00000002*	*0.00000002*	*0.00000001*	*0.00000002*
Normalized composition without impurities						
Methane	97.2362	0.0020	87.5221	0.0023	77.7982	0.0023
Hydrogen	–	–	9.9928	0.0031	19.9946	0.0046
Nitrogen	1.40097	0.00028	1.25838	0.00024	1.11842	0.00027
Carbon dioxide	0.361460	0.000113	0.324953	0.000092	0.288529	0.000084
Ethane	0.398705	0.000033	0.360839	0.000031	0.320307	0.000031
Propane	0.201221	0.000020	0.180328	0.000019	0.160279	0.000019
n-Butane	0.100398	0.000052	0.090235	0.000047	0.079774	0.000042
Isobutane	0.100431	0.000023	0.090531	0.000021	0.079823	0.000019
n-Pentane	0.050072	0.000023	0.045181	0.000021	0.040107	0.000019
Isopentane	0.049928	0.000023	0.045043	0.000021	0.040017	0.000019
Neopentane	0.050782	0.000022	0.044754	0.000020	0.039945	0.000018
n-Hexane	0.049883	0.000018	0.044883	0.000016	0.040092	0.000015
Molar mass, M / (g/mol)	16.628		15.167		13.705	
Normalized density, ρ_n / (kg/m^3)	0.70468		0.64248		0.58032	
Higher Heating Value, *HHV* / (MJ/m^3)	37.749		35.174		32.598	
Wobbe index, W_s / (MJ/m^3)	49.783		48.580		47.373	

% with respect to the values for the original H_2-free natural gas mixture (G 431), when 10 % (G 453) or 20 % (G 454) of hydrogen is added. The variation in the Wobbe index is less pronounced, decreasing only by 2.5 % and 5 %, respectively.

The T, p coordinate of the critical point of the H_2-free natural gas mixture (G 431) is (197.2 K, 5.4 MPa), with the corresponding cricondentherm at (247.9 K, 3.9 MPa), and the cricondenbar at (225.7 K, 7.5 MPa). Similarly, for the mixture G 453 (G 431 + 10 % H_2), the critical point is at (176.1 K, 4.3 MPa), the cricondentherm at (247.4 K, 4.3 MPa), and the cricondenbar at (219.3 K, 9.2 MPa). Finally, for the mixture G 454 (G 431 + 20 % H_2), the critical point is at (160.2 K, 3.9 MPa) the cricondentherm at (246.9 K, 4.9 MPa), and the cricondenbar at (207.4 K, 11.8 MPa). Note that neopentane is not included in any of the mixture models used in this work, thus it had to be added to the concentration of *n*-pentane.

2.2. Equipment and measurement procedure description

The experimental part of this work is accomplished with a single-sinker magnetic suspension densimeter. It consists of a pressurized diamagnetic CuCrZr cell containing a monocrystalline silicon sinker of calibrated volume (V_s = 226.4440 ± 0.0026 cm^3) surrounded by the sample gas. The buoyancy force is transmitted to an analytical microbalance (XPE205DR, Mettler Toledo GmbH) located above the cell at ambient pressure through a magnetic coupling device. This kind of setup is currently regarded as the most accurate to determine fluid density over a large range of temperatures and pressures, providing an absolute determination of the density without the need for calibration fluids. The principles of measurement were developed by Kleinrahm, Wagner, and Lösch [31–33], originally with two-sinker devices (improved accuracy, especially at low density, mainly due to compensation for adsorption effects, which may be relevant at very low density) and then with single-sinker devices (less complex but equally accurate at high density [34,35]).

The working equation is:

$$\rho_{\mathrm{fluid}} = \frac{\varphi_0 m_s + (m_{\mathrm{Ti}} - m_{\mathrm{Ta}}) + (W_{\mathrm{ZP}} - W_{\mathrm{MP}})/\alpha}{V_s(T,p)} \frac{1}{\varphi_0} + \frac{\varepsilon_\rho}{\varphi_0}\frac{\chi_s}{\chi_{s0}}\left(\frac{\rho_s}{\rho_0} - \frac{\rho_{\mathrm{fluid}}}{\rho_0}\right)\rho_{\mathrm{fluid}} \quad (1)$$

where the subscripts fluid, s, Ti, Ta, ZP, and MP stand for the fluid, sinker ("specific" in case of χ_s and χ_{s0}), titanium and tantalum compensation masses, zero and measuring positions of the magnetic coupling, while the terms m, V, and ρ denote the mass, volume, and density, respectively.

α is the so-called *calibration factor* determined by weighing two calibrated compensation masses of tantalum and titanium, alternatively placed in the upper pan of the microbalance by means of an automatically controlled changing device. Both compensation masses have nearly the same volume and their mass difference is close to the mass of the sinker. In this way, the balance is always operated near its zero position, avoiding measurement errors that originate from the non-linearity of the balance itself.

The magnetic coupling system is composed of two magnets separated

Table 3
Contributions to the overall expanded ($k = 2$) uncertainty in density, U_T (ρ_{exp}), for the three reference natural gas mixtures studied in this work.

Source	Contribution ($k = 2$)	Units	Estimation in density ($k = 2$)	
			kg·m^{-3}	%
G 431				
Temperature, T	0.015	K	<0.0080	<0.0049
Pressure, p	<0.005	MPa	(0.021–0.068)	(0.018–0.37)
Composition, x_i	<0.0004	mol·mol^{-1}	<0.0012	<0.0014
Density, ρ	(0.024–0.048)	kg·m^{-3}	(0.024–0.048)	(0.022–0.41)
Sum			(0.031–0.078)	(0.028–0.54)
G 453 (G 431 + 10 % H_2)				
Temperature, T	0.015	K	<0.0059	<0.0038
Pressure, p	<0.005	MPa	(0.019–0.051)	(0.022–0.37)
Composition, x_i	<0.0004	mol·mol^{-1}	<0.014	<0.0084
Density, ρ	(0.023–0.043)	kg·m^{-3}	(0.023–0.043)	(0.024–0.45)
Sum			(0.030–0.064)	(0.034–0.57)
G 454 (G 431 + 20 % H_2)				
Temperature, T	0.015	K	<0.0045	<0.0032
Pressure, p	<0.005	MPa	(0.017–0.040)	(0.021–0.37)
Composition, x_i	<0.0004	mol·mol^{-1}	<0.015	<0.0099
Density, ρ	(0.023–0.041)	kg·m^{-3}	(0.023–0.041)	(0.026–0.49)
Sum			(0.029–0.055)	(0.034–0.61)

by the upper cell wall: an electromagnet hanging from the lower hook of the balance and a permanent magnet attached to the upper end of the sinker support inside the cell. The actual measuring procedure is carried out in a differential manner, in the zero position (ZP) the electromagnet only attracts the sinker support without lifting the sinker, whereas in the measuring position (MP) a higher force is exerted on the permanent magnet which also lifts the silicon sinker. The difference between the readings of the balance, W, in these two positions allows for cancelling the weights of the sinker support, the magnets, and the balance hook, which consequently minimizes systematic errors.

Due to the fact that the vertical positions of the ZP and MP are not exactly the same, together with other possible instabilities in the alignment of the magnets during the measuring procedure, the density determination should be corrected for the *force transmission error*. This perturbation is divided into two terms: the apparatus-specific effect and the fluid-specific effect. The apparatus-specific effect is accounted in Equation (1) by φ_0 and determined by measuring the sinker in vacuum after each isotherm is finished. Neglecting this correcting term can lead to significant errors [36], therefore, it must always be considered. The fluid-specific effect is described in Equation (1) by the second term on the right side and depends (a) on the specific magnetic susceptibility of the fluid χ_s (note that here, the subscript *s* stands for *specific* and not for *sinker*), (b) the so-called apparatus-specific constant ε_ρ, and (c) the reducing constants $\chi_{s0} = 10^{-8}$ m^3 kg^{-1} and $\rho_0 = 1000$ kg m^{-3}. The value of ε_ρ was estimated for our apparatus as a function of temperature and density in a previous work by two different methods [37]. Contrary to the apparatus-specific effect, the fluid-specific effect is less significant for diamagnetic fluids, but leads to relative errors of up to 3 % for paramagnetic fluids (since χ_s for paramagnetic fluids, which is temperature dependent, can be 100 times stronger compared to diamagnetic fluids) [38–40].

The pressure of the fluid is determined by two quartz crystal transducers: one for the low-pressure range from (0–3) MPa (Digiquartz 2300A-101, Paroscientific Inc.) and the other for the higher pressures in the range between (3–20) MPa (Digiquartz 43 KR-HHT-101, Paroscientific Inc.). The estimated expanded ($k = 2$) uncertainty is $U(p) = (7.5{\cdot}10^{-5}\ (p/\text{MPa}) + 3.5{\cdot}10^{-3})$ MPa for the high-pressure transducer, and $U(p) = (6.0{\cdot}10^{-5}\ (p/\text{MPa}) + 1.7{\cdot}10^{-3})$ MPa for the low-pressure transducer.

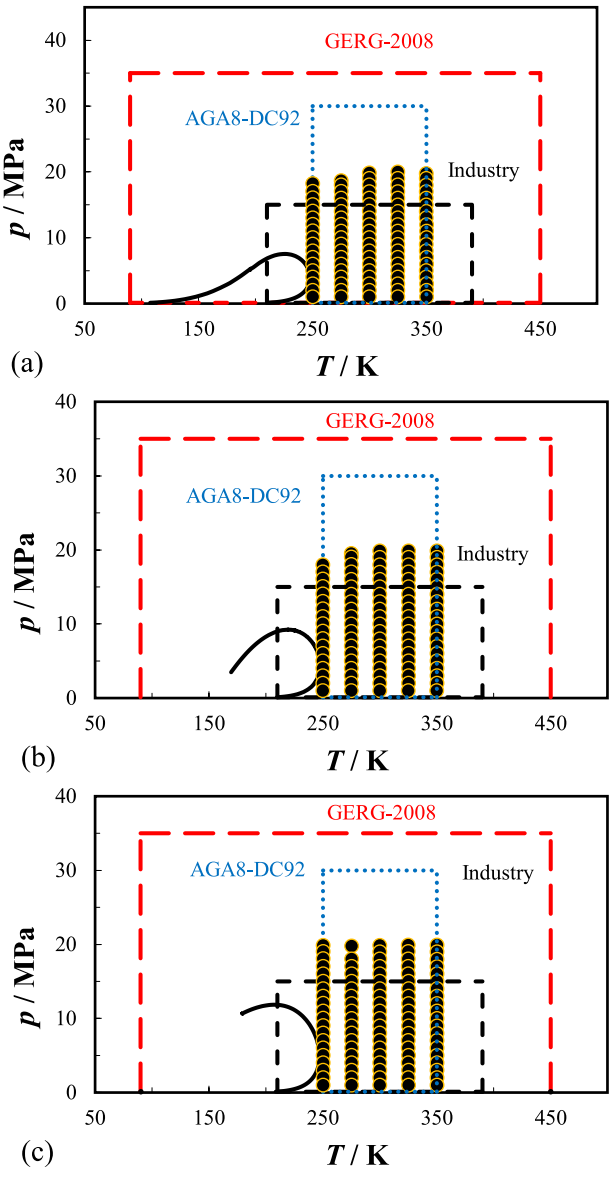

Fig. 1. p, T-phase diagram showing the experimental points measured (●) and the calculated phase envelope (solid line) using the improved-GERG EoS [44–46] for: a) (H_2-free) natural gas mixture G 431, b) (H_2-enriched) natural gas mixture G 453 (G 431 + 10 % H_2), and c) (H_2-enriched) natural gas mixture G 454 (G 431 + 20 % H_2), respectively. The marked temperature and pressure ranges represent the range of validity of the AGA8-DC92 EoS [19] (blue dotted line) and GERG-2008 EoS [20,21] (red dashed line), and the area of interest for the gas industry (black dashed line). (For interpretation of the references to colour in this figure legend, the reader is referred to the Web version of this article.)

The temperature of the cell, thermostated by means of an oil thermal bath (Dyneo DD-1000F, Julabo GmbH) and an electrical heating cylinder around the cell connected to a temperature controller (MC-E, Julabo GmbH) is measured by two standard platinum resistance thermometers SPRT-25 (S1059PJ5X6, Minco Products Inc.) controlled by an AC resistance bridge (ASL F700, Automatic Systems Laboratory). The estimated expanded ($k = 2$) uncertainty in temperature is $U(T) = 0.015$ K.

A more detailed description of our equipment and the measurement procedure can be found in our previous papers [41,42].

Table 4
Experimental (p, ρ_{exp}, T) measurements for the (H_2-free) natural gas mixture G 431, absolute and relative expanded ($k = 2$) uncertainty in density, U (ρ_{exp}), relative deviations from the density given by the AGA8-DC92 EoS [19], $\rho_{AGA8\text{-}DC92}$, the GERG-2008 EoS [20,21], $\rho_{GERG\text{-}2008}$, and the improved-GERG-2008 EoS [44–46], $\rho_{GERG\text{-}improved}$.

T/K[a]	p/MPa[a]	ρ_{exp}/(kg·m^{-3})[(a)]	U (ρ_{exp})/(kg·m^{-3})	10^2 U (ρ_{exp})/ρ_{exp}	10^2 (ρ_{exp} − $\rho_{AGA8\text{-}DC92}$)/$\rho_{AGA8\text{-}DC92}$	10^2 (ρ_{exp} − $\rho_{GERG\text{-}2008}$)/$\rho_{GERG\text{-}2008}$	10^2 (ρ_{exp} − $\rho_{GERG\text{-}improved}$)/$\rho_{GERG\text{-}improved}$
250.000 K							
250.133	18.23491	219.356	0.048	0.022	−0.053	0.049	<0.001
250.133	17.04296	209.224	0.047	0.022	−0.048	0.041	−0.002
250.133	16.04613	199.707	0.046	0.023	−0.044	0.032	−0.009
250.132	15.04764	189.084	0.044	0.023	−0.038	0.023	−0.019
250.133	14.04021	177.147	0.043	0.024	−0.029	0.018	−0.028
250.132	13.03555	163.969	0.042	0.025	−0.028	0.013	−0.036
250.130	12.03305	149.638	0.040	0.027	−0.033	0.016	−0.034
250.130	11.03005	134.394	0.038	0.028	−0.030	0.034	−0.007
250.130	10.02337	118.610	0.036	0.031	−0.036	0.037	0.013
250.132	9.01924	102.948	0.035	0.034	−0.028	0.045	0.038
250.132	8.01383	87.817	0.033	0.037	−0.023	0.046	0.049
250.133	7.01058	73.591	0.031	0.042	−0.020	0.047	0.051
250.132	6.00807	60.385	0.030	0.049	−0.026	0.038	0.040
250.132	5.00596	48.212	0.028	0.059	−0.035	0.026	0.026
250.132	4.00437	37.010	0.027	0.073	−0.044	0.010	0.008
250.130	3.00344	26.689	0.026	0.097	−0.054	−0.010	−0.013
250.130	2.00266	17.146	0.025	0.145	−0.046	−0.016	−0.019
250.129	1.00225	8.287	0.024	0.287	0.004	0.021	0.018
275.000 K							
275.108	18.67854	181.509	0.044	0.024	−0.016	0.043	−0.004
275.108	18.04554	176.201	0.043	0.024	−0.011	0.043	−0.003
275.106	17.02865	167.199	0.042	0.025	−0.010	0.039	−0.006
275.107	16.03037	157.800	0.041	0.026	−0.008	0.038	−0.003
275.107	15.02829	147.828	0.040	0.027	−0.008	0.038	0.001
275.108	14.02385	137.348	0.039	0.028	−0.010	0.038	0.007
275.108	13.01897	126.477	0.037	0.029	−0.009	0.041	0.017
275.109	12.01820	115.381	0.036	0.031	−0.009	0.041	0.025
275.108	11.01837	104.183	0.035	0.033	<0.001	0.048	0.039
275.107	10.01895	93.003	0.033	0.036	−0.002	0.045	0.041
275.108	9.01383	81.928	0.032	0.039	−0.002	0.045	0.044
275.107	8.00999	71.145	0.031	0.044	−0.003	0.044	0.043
275.107	7.00835	60.751	0.030	0.049	−0.002	0.044	0.044
275.106	6.00705	50.773	0.029	0.056	−0.005	0.039	0.038
275.103	5.00540	41.236	0.028	0.067	−0.006	0.034	0.032
275.105	4.00342	32.143	0.027	0.083	−0.005	0.029	0.026
275.104	3.00300	23.504	0.026	0.109	−0.004	0.023	0.019
275.104	2.00213	15.283	0.025	0.161	0.011	0.029	0.025
275.106	1.00227	7.467	0.024	0.318	0.038	0.048	0.045
300.000 K							
300.069	19.83028	160.549	0.041	0.026	0.005	0.041	<0.001
300.066	19.00896	154.521	0.040	0.026	0.003	0.038	<0.001
300.061	18.00697	146.887	0.040	0.027	<0.001	0.037	0.001
300.060	17.00683	138.967	0.039	0.028	−0.003	0.035	0.003
300.049	16.01803	130.872	0.038	0.029	−0.011	0.029	0.001
300.057	15.01473	122.419	0.037	0.030	−0.008	0.034	0.009
300.052	14.04309	114.049	0.036	0.031	−0.012	0.031	0.010
300.059	13.00805	104.984	0.035	0.033	−0.008	0.035	0.018
300.057	12.00698	96.131	0.034	0.035	−0.009	0.033	0.020
300.066	11.00670	87.265	0.033	0.038	<0.001	0.042	0.032
300.064	10.00708	78.432	0.032	0.041	−0.004	0.037	0.029
300.072	9.00658	69.682	0.031	0.044	−0.001	0.038	0.032
300.074	8.00637	61.071	0.030	0.049	<0.001	0.037	0.033
300.073	7.00541	52.630	0.029	0.055	0.002	0.037	0.034
300.072	6.00469	44.394	0.028	0.063	0.002	0.033	0.030
300.072	5.00421	36.387	0.027	0.074	0.004	0.031	0.029
300.067	4.00390	28.621	0.026	0.091	0.003	0.025	0.022
300.068	3.00496	21.112	0.025	0.120	0.009	0.026	0.022
300.071	2.00279	13.828	0.024	0.177	0.021	0.033	0.029
300.069	1.00325	6.807	0.024	0.347	0.027	0.035	0.031
325.000 K							
325.063	20.00253	140.124	0.039	0.028	0.008	0.042	0.006
325.065	19.02061	133.677	0.038	0.029	0.005	0.041	0.007
325.063	18.01414	126.885	0.037	0.029	<0.001	0.038	0.007
325.063	17.01119	119.948	0.037	0.030	−0.004	0.036	0.007
325.064	16.00759	112.859	0.036	0.032	−0.005	0.036	0.010
325.065	15.00686	105.660	0.035	0.033	−0.008	0.034	0.011
325.065	14.00756	98.370	0.034	0.035	−0.010	0.033	0.012
325.063	13.00645	90.995	0.033	0.037	−0.010	0.031	0.014
325.064	12.00582	83.578	0.032	0.039	−0.010	0.030	0.015
325.064	11.00642	76.158	0.032	0.041	−0.004	0.034	0.022

(*continued on next page*)

Table 4 (*continued*)

T/K[a]	p/MPa[a]	ρ_{exp}/(kg·m^{-3})[(a)]	$U(\rho_{exp})$/(kg·m^{-3})	$10^2\,U(\rho_{exp})/\rho_{exp}$	$10^2(\rho_{exp}-\rho_{AGA8\text{-}DC92})/\rho_{AGA8\text{-}DC92}$	$10^2(\rho_{exp}-\rho_{GERG\text{-}2008})/\rho_{GERG\text{-}2008}$	$10^2(\rho_{exp}-\rho_{GERG\text{-}improved})/\rho_{GERG\text{-}improved}$
325.063	10.00509	68.733	0.031	0.045	−0.006	0.029	0.020
325.064	9.00636	61.370	0.030	0.049	−0.004	0.028	0.022
325.065	8.00457	54.051	0.029	0.054	−0.003	0.026	0.021
325.063	7.00428	46.834	0.028	0.060	0.001	0.026	0.023
325.064	6.00536	39.734	0.027	0.069	0.003	0.025	0.023
325.063	5.00332	32.737	0.027	0.081	0.004	0.022	0.020
325.064	4.00301	25.888	0.026	0.100	0.002	0.018	0.015
325.066	3.00225	19.184	0.025	0.131	0.005	0.017	0.014
325.067	2.00329	12.644	0.024	0.192	0.011	0.020	0.016
325.069	1.00007	6.234	0.024	0.378	0.027	0.034	0.030
350.000 K							
350.055	19.75548	122.747	0.037	0.030	0.005	0.045	0.010
350.060	19.00598	118.326	0.036	0.031	0.001	0.042	0.009
350.062	18.00664	112.330	0.036	0.032	−0.004	0.039	0.008
350.065	17.00571	106.218	0.035	0.033	−0.007	0.036	0.008
350.070	16.00649	100.022	0.034	0.034	−0.007	0.036	0.010
350.069	15.00496	93.728	0.034	0.036	−0.010	0.032	0.009
350.069	14.00607	87.384	0.033	0.038	−0.010	0.030	0.011
350.071	13.00542	80.977	0.032	0.040	−0.009	0.029	0.013
350.074	12.00550	74.541	0.031	0.042	−0.008	0.028	0.015
350.074	11.00471	68.085	0.031	0.045	<0.001	0.033	0.023
350.074	10.00535	61.630	0.030	0.049	−0.002	0.027	0.020
350.073	9.00492	55.186	0.029	0.053	−0.001	0.025	0.020
350.071	8.00374	48.769	0.028	0.058	0.001	0.024	0.021
350.074	7.00271	42.398	0.028	0.065	0.005	0.025	0.023
350.074	6.00345	36.095	0.027	0.075	0.005	0.023	0.021
350.072	5.00322	29.857	0.026	0.088	0.005	0.021	0.019
350.073	4.00241	23.695	0.026	0.108	0.008	0.021	0.019
350.075	3.00359	17.634	0.025	0.141	0.009	0.020	0.017
350.077	2.00208	11.651	0.024	0.208	0.004	0.013	0.010
350.080	1.00190	5.779	0.024	0.407	0.025	0.031	0.028

[a] Expanded uncertainties ($k = 2$): $U(p > 3)/\mathrm{MPa} = 75{\cdot}10^{-6}{\cdot}\frac{p}{\mathrm{MPa}} + 3.5{\cdot}10^{-3}$; $U(p < 3)/\mathrm{MPa} = 60{\cdot}10^{-6}{\cdot}\frac{p}{\mathrm{MPa}} + 1.7{\cdot}10^{-3}$; $U(T) = 15$ mK; $\frac{U(\rho)}{\mathrm{kg{\cdot}m^{-3}}} = 2.5{\cdot}10^{4}\frac{\chi_S}{\mathrm{m^3kg^{-1}}} + 1.1{\cdot}10^{-4}{\cdot}\frac{\rho}{\mathrm{kg{\cdot}m^{-3}}} + 2.3{\cdot}10^{-2}$.

3. Experimental results

3.1. Uncertainty of the measurements

The experimental overall expanded ($k = 2$) uncertainty $U_T(\rho_{exp})$ for the density measurements is reported in Table 3 in both absolute and relative terms. It takes into account the contributions from the uncertainty of the density determination, $U(\rho_{exp})$, which has been thoroughly evaluated as a function of density and specific magnetic susceptibility in two previous works for our single-sinker densimeter [37,42]:

$$U(\rho_{exp})/(\mathrm{kg{\cdot}m^{-3}}) = 2.5{\cdot}10^{4}{\cdot}\chi_s/(\mathrm{m^3{\cdot}kg^{-1}}) + 1.1{\cdot}10^{-4}{\cdot}\rho_{exp}/(\mathrm{kg{\cdot}m^{-3}}) + 2.3{\cdot}10^{-2} \quad (2)$$

combined with the uncertainties from pressure, $u(p)$, temperature, $u(T)$, and composition, $u(x_i)$, following the law of uncertainty propagation [28,43]:

$$U_T(\rho_{exp}) = 2\left[u(\rho_{exp})^2 + \left(\left.\frac{\partial\rho}{\partial p}\right|_{T,x}u(p)\right)^2 + \left(\left.\frac{\partial\rho}{\partial T}\right|_{p,x}u(T)\right)^2 + \sum_i\left(\left.\frac{\partial\rho}{\partial x_i}\right|_{T,p,x_j\neq x_i}u(x_i)\right)^2\right]^{0.5} \quad (3)$$

where the partial derivatives of the mixture density with respect to pressure and temperature are estimated with the REFPROP 10 software [29,30] using the improved-GERG-2008 EoS [44–46]. The most significant term is due to $U(\rho_{exp})$, with values up to 0.05 kg m^{-3} (0.5 %), closely followed by $U(p)$, and then with minor contributions from $U(x_i)$ and $U(T)$, below 0.015 kg m^{-3} (0.01 %). The overall experimental expanded ($k = 2$) uncertainty for the three mixtures ranges from (0.029–0.078) kg·m^{-3}, i.e., from (0.028–0.61) %.

3.2. Density measurements

The measured points of the three studied mixtures are represented in the p,T plots of Fig. 1, together with the saturation curves estimated from the improved-GERG-2008 EoS, the ranges of interest for the gas industry at pipeline conditions, and the approved application ranges of the AGA8-DC92 EoS and GERG-2008 EoS. Measurements were carried out at five temperatures, (250, 275, 300, 325, and 350) K, in decreasing pressure steps of 1 MPa starting from 20 MPa down to 1 MPa. Tables 4–6 list the experimental (p, ρ, T) data for the G 431 (H_2-free high calorific natural gas), G 453 (G 431 + 10 % H_2), and G 454 (G432 + 20 % H_2) mixtures, respectively, with the corresponding compositions reported in Table 2.

Tables 4–6 also display the experimental expanded ($k = 2$) uncertainty in density, estimated by Equation (3), in absolute terms and as a percentage, as well as the relative deviations of the experimental density from the calculated values with the AGA8-DC92 EoS, GERG-2008 EoS, and improved-GERG-2008 EoS.

Table 5
Experimental (p, ρ_{exp}, T) measurements for the (H_2-enriched) natural gas mixture G 453 (G 431 + 10 % H_2), absolute and relative expanded ($k = 2$) uncertainty in density, U (ρ_{exp}), relative deviations from the density given by the AGA8-DC92 EoS [19], $\rho_{AGA8\text{-}DC92}$, the GERG-2008 EoS [20,21], $\rho_{GERG\text{-}2008}$, and the improved-GERG-2008 EoS [44–46], $\rho_{GERG\text{-}improved}$.

T/K[a]	p/MPa[a]	ρ_{exp}/(kg·m^{-3})[(a)]	U (ρ_{exp})/(kg·m^{-3})	10^2 U (ρ_{exp})/ρ_{exp}	10^2 (ρ_{exp} − $\rho_{AGA8\text{-}DC92}$)/$\rho_{AGA8\text{-}DC92}$	10^2 (ρ_{exp} − $\rho_{GERG\text{-}2008}$)/$\rho_{GERG\text{-}2008}$	10^2 (ρ_{exp} − $\rho_{GERG\text{-}improved}$)/$\rho_{GERG\text{-}improved}$
250.000 K							
250.038	17.99536	178.985	0.043	0.024	−0.189	−0.181	−0.002
250.037	17.03752	170.862	0.042	0.025	−0.157	−0.179	−0.055
250.036	16.07095	162.081	0.041	0.026	−0.126	−0.173	−0.107
250.036	15.06005	152.263	0.040	0.026	−0.095	−0.161	−0.152
250.035	14.05220	141.856	0.039	0.028	−0.067	−0.142	−0.184
250.037	13.04991	130.960	0.038	0.029	−0.043	−0.116	−0.199
250.036	12.03622	119.509	0.036	0.031	−0.024	−0.086	−0.199
250.037	11.01667	107.723	0.035	0.033	−0.005	−0.047	−0.181
250.037	10.02226	96.137	0.034	0.035	−0.003	−0.020	−0.168
250.037	9.01596	84.522	0.033	0.038	−0.009	0.002	−0.155
250.038	8.01353	73.224	0.031	0.043	−0.022	0.016	−0.144
250.038	7.00732	62.285	0.030	0.048	−0.037	0.024	−0.133
250.039	6.00617	51.876	0.029	0.055	−0.056	0.020	−0.127
250.041	5.00456	41.980	0.028	0.066	−0.074	0.007	−0.123
250.038	4.00336	32.615	0.027	0.082	−0.090	−0.013	−0.122
250.038	2.98984	23.663	0.026	0.108	−0.071	−0.005	−0.089
250.037	2.00040	15.401	0.025	0.160	−0.041	0.007	−0.050
250.041	1.00007	7.500	0.024	0.316	0.088	0.115	0.085
275.000 K							
275.040	19.52291	158.425	0.041	0.026	−0.092	−0.077	−0.058
275.041	19.06379	155.138	0.041	0.026	−0.087	−0.076	−0.065
275.042	18.04784	147.614	0.040	0.027	−0.075	−0.074	−0.079
275.041	17.03708	139.792	0.039	0.028	−0.065	−0.072	−0.088
275.041	16.03514	131.721	0.038	0.029	−0.057	−0.069	−0.094
275.041	15.03326	123.370	0.037	0.030	−0.048	−0.064	−0.095
275.042	14.02489	114.721	0.036	0.031	−0.041	−0.057	−0.094
275.042	13.02105	105.923	0.035	0.033	−0.035	−0.050	−0.093
275.041	12.01916	97.016	0.034	0.035	−0.033	−0.044	−0.093
275.040	11.01746	88.058	0.033	0.037	−0.027	−0.031	−0.087
275.040	10.01451	79.091	0.032	0.040	−0.031	−0.027	−0.090
275.040	9.01211	70.208	0.031	0.044	−0.035	−0.021	−0.090
275.040	8.00822	61.445	0.030	0.049	−0.041	−0.017	−0.091
275.042	7.00789	52.898	0.029	0.055	−0.042	−0.010	−0.086
275.042	6.00482	44.545	0.028	0.063	−0.046	−0.009	−0.082
275.041	5.00325	36.450	0.027	0.074	−0.048	−0.009	−0.077
275.041	4.00231	28.623	0.026	0.091	−0.045	−0.007	−0.066
275.040	2.98906	20.977	0.025	0.120	−0.026	0.007	−0.040
275.041	2.00066	13.782	0.024	0.177	−0.007	0.018	−0.016
275.040	1.00071	6.767	0.024	0.349	0.039	0.054	0.035
300.000 K							
300.080	19.86739	137.734	0.039	0.028	−0.021	−0.012	−0.017
300.079	19.01352	132.264	0.038	0.029	−0.019	−0.013	−0.017
300.080	18.01111	125.661	0.037	0.030	−0.017	−0.012	−0.016
300.078	17.01112	118.891	0.036	0.031	−0.016	−0.013	−0.015
300.078	16.01481	111.982	0.036	0.032	−0.014	−0.013	−0.014
300.078	15.01186	104.882	0.035	0.033	−0.014	−0.013	−0.014
300.078	14.01252	97.691	0.034	0.035	−0.011	−0.011	−0.014
300.079	13.00993	90.386	0.033	0.037	−0.010	−0.009	−0.015
300.078	12.00725	83.021	0.032	0.039	−0.009	−0.007	−0.017
300.078	11.00800	75.658	0.031	0.042	−0.003	<0.001	−0.016
300.078	10.00623	68.274	0.031	0.045	−0.006	0.001	−0.021
300.079	9.00729	60.948	0.030	0.049	−0.006	0.003	−0.024
300.078	8.00532	53.664	0.029	0.054	−0.006	0.006	−0.025
300.078	7.00595	46.488	0.028	0.061	−0.004	0.011	−0.023
300.077	6.00506	39.409	0.027	0.069	−0.005	0.012	−0.022
300.076	5.00463	32.462	0.027	0.082	−0.005	0.013	−0.020
300.077	4.00398	25.655	0.026	0.101	−0.004	0.014	−0.017
300.078	3.00382	19.004	0.025	0.132	−0.001	0.015	−0.011
300.076	2.00305	12.509	0.024	0.194	0.005	0.018	−0.001
300.076	1.00193	6.175	0.024	0.382	0.018	0.027	0.016
325.000 K							
325.081	19.89360	121.127	0.037	0.030	−0.023	−0.012	−0.004
325.082	19.01219	116.089	0.036	0.031	−0.024	−0.013	−0.001
325.081	18.01151	110.255	0.035	0.032	−0.025	−0.015	<0.001
325.084	17.01191	104.312	0.035	0.033	−0.024	−0.015	0.002
325.082	16.01309	98.270	0.034	0.035	−0.026	−0.018	<0.001
325.081	15.01025	92.117	0.033	0.036	−0.025	−0.018	<0.001
325.081	14.00797	85.892	0.033	0.038	−0.024	−0.018	−0.002
325.081	13.00865	79.626	0.032	0.040	−0.022	−0.017	−0.004
325.081	12.00826	73.311	0.031	0.043	−0.022	−0.018	−0.008

(*continued on next page*)

Table 5 (*continued*)

T/K[a]	p/MPa[a]	ρ_{exp}/(kg·m^{-3})[(a)]	U (ρ_{exp})/(kg·m^{-3})	10^2 U (ρ_{exp})/ρ_{exp}	10^2 (ρ_{exp} − $\rho_{AGA8\text{-}DC92}$)/$\rho_{AGA8\text{-}DC92}$	10^2 (ρ_{exp} − $\rho_{GERG\text{-}2008}$)/$\rho_{GERG\text{-}2008}$	10^2 (ρ_{exp} − $\rho_{GERG\text{-}improved}$)/$\rho_{GERG\text{-}improved}$
325.079	11.00604	66.966	0.031	0.046	−0.015	−0.011	−0.006
325.081	10.00712	60.628	0.030	0.049	−0.015	−0.011	−0.010
325.080	9.00677	54.294	0.029	0.054	−0.015	−0.010	−0.014
325.079	8.00716	47.990	0.028	0.059	−0.016	−0.010	−0.018
325.079	7.00597	41.721	0.028	0.066	−0.013	−0.007	−0.017
325.081	6.00383	35.499	0.027	0.076	−0.016	−0.008	−0.021
325.082	5.00406	29.362	0.026	0.089	−0.017	−0.009	−0.022
325.084	4.00309	23.297	0.026	0.110	−0.019	−0.011	−0.024
325.084	3.00294	17.324	0.025	0.143	−0.033	−0.024	−0.036
325.084	2.00276	11.450	0.024	0.211	−0.038	−0.030	−0.039
325.077	1.00145	5.672	0.024	0.415	−0.041	−0.034	−0.040
350.000 K							
350.077	19.87136	108.394	0.035	0.032	−0.022	−0.009	0.012
350.079	19.00817	103.959	0.035	0.033	−0.023	−0.010	0.013
350.078	18.00707	98.733	0.034	0.035	−0.026	−0.013	0.013
350.079	17.00650	93.431	0.034	0.036	−0.026	−0.014	0.013
350.079	16.00701	88.062	0.033	0.037	−0.025	−0.015	0.014
350.077	15.00673	82.624	0.032	0.039	−0.025	−0.016	0.012
350.075	14.00468	77.121	0.032	0.041	−0.024	−0.017	0.009
350.075	13.00594	71.590	0.031	0.043	−0.022	−0.017	0.007
350.075	12.00520	66.012	0.030	0.046	−0.020	−0.016	0.005
350.074	11.00582	60.421	0.030	0.049	−0.012	−0.009	0.008
350.075	10.00544	54.804	0.029	0.053	−0.013	−0.011	0.003
350.074	9.00462	49.183	0.028	0.058	−0.013	−0.011	−0.001
350.073	8.00495	43.575	0.028	0.064	−0.014	−0.012	−0.005
350.075	7.00384	37.977	0.027	0.072	−0.009	−0.006	−0.002
350.075	6.00276	32.405	0.027	0.082	−0.011	−0.007	−0.005
350.076	5.00261	26.873	0.026	0.096	−0.011	−0.007	−0.007
350.075	4.00245	21.385	0.025	0.118	−0.015	−0.009	−0.011
350.075	3.00247	15.949	0.025	0.155	−0.022	−0.016	−0.019
350.074	2.00193	10.569	0.024	0.228	−0.028	−0.022	−0.025
350.072	1.00211	5.257	0.023	0.446	−0.014	−0.008	−0.011

[a] Expanded uncertainties ($k = 2$): $U(p > 3)/\text{MPa} = 75{\cdot}10^{-6}{\cdot}\frac{p}{\text{MPa}} + 3.5{\cdot}10^{-3}$; $U(p < 3)/\text{MPa} = 60{\cdot}10^{-6}{\cdot}\frac{p}{\text{MPa}} + 1.7{\cdot}10^{-3}$; $U(T) = 15$ mK; $\frac{U(\rho)}{\text{kg·m}^{-3}} = 2.5{\cdot}10^{4}\frac{\chi_S}{\text{m}^3\text{kg}^{-1}} + 1.1{\cdot}10^{-4}{\cdot}\frac{\rho}{\text{kg·m}^{-3}} + 2.3{\cdot}10^{-2}$.

AGA8-DC92 EoS [19] is the reference mixture model from the *American Gas Association (AGA)*. This equation was initially formulated as a virial expansion series of the compressibility factor of fluid mixtures and then recast as an explicit form of the Helmholtz energy to also account for the calorific properties in addition to volumetric ones [47]. Its application range is restricted to homogeneous gas and supercritical phases in the temperature ranges from (250–350) K and pressures up to 30 MPa.

Its – nowadays in Europe more widespread – counterpart is the GERG-2008 EoS [20,21] from the *Groupe Européen de Recherches Gazières (GERG)*, which was extended to also cover the liquid and vapor-liquid equilibria (VLE) regions, covering the ranges from (60–700) K and up to 70 MPa [44]. Both multiparametric models were developed to describe the thermophysical properties of natural gas mixtures, including 21 components (C_1 to C_{10}, and additionally iso-C_4 and iso-C_5, N_2, CO_2, CO, H_2O, O_2, H_2, Ar, He, and H_2S), at pipeline conditions. The accuracy of the EoS is directly determined by the availability and uncertainty of the experimental VLE, density, speed of sound, enthalpy differences, and heat capacity databases.

Two major modifications to the GERG mixture model, taking the formulation of the GERG-2008 EoS as a basic framework, were subsequently implemented based on more comprehensive and consolidated experimental data as well as on new modified fitting techniques. The application ranges of temperature, pressure, and composition were not modified. The first modification focused on meeting the demand for the accurate calculation of thermophysical properties in the subcooled liquid region between (90–180) K with pressures of up to 10 MPa from the liquefied natural gas (LNG) industry [45]. Thus, new binary specific departure functions for (methane + *n*-pentane) and (methane + isopentane) were developed and the departure functions for the binaries (methane + *n*-butane) and (methane + isobutane) were reparametrized. In this way, it became possible to reproduce the density measurements of LNG-type mixtures within their experimental uncertainty [48,49], whereas the calorific properties representation was also improved with respect to the original GERG-2008 EoS.

The second modification was adopted to improve the accurate description of the thermophysical properties for hydrogen-rich multicomponent mixtures in the wider temperature, pressure, and composition ranges of processes involved in the hydrogen economy [46]. For this purpose, the first step was to switch from the original pure-fluid equations from GERG-2008 EoS to the current reference pure-fluid equations. Then, three new binary specific departure functions were developed for the binary systems ($N_2 + H_2$), ($CO_2 + H_2$), and ($CO + H_2$), whereas the original specific departure function for the binary system ($CH_4 + H_2$) was reparametrized. The most significant improvement, however, was the correction of the unphysical behavior for the predicted phase envelope from the GERG-2008 EoS at temperatures lower than 120 K for the binary system ($CH_4 + H_2$), lower than 100 K for the ($N_2 + H_2$), 80 K for the ($CO + H_2$), and lower than 260 K for the ($CO_2 + H_2$). At these states, the original GERG-2008 EoS produces an open phase envelope, which means a liquid-liquid equilibrium, contradicting the experimental data available. Apart from fixing these artifacts, the differences with experimental VLE, homogeneous density and speed of sound data were significantly reduced in several cases or, at least, remained similar to that of GERG-2008 EoS for the remaining fluid regions. In this work, we denote the modified GERG model with the two above described adjustments as improved-GERG-2008 EoS.

Table 6
Experimental (p, ρ_{exp}, T) measurements for the (H_2-enriched) natural gas mixture G 454 (G 431 + 20 % H_2), absolute and relative expanded ($k = 2$) uncertainty in density, U (ρ_{exp}), relative deviations from the density given by the AGA8-DC92 EoS [19], $\rho_{AGA8\text{-}DC92}$, the GERG-2008 EoS [20,21], $\rho_{GERG\text{-}2008}$, and the improved-GERG-2008 EoS [44–46], $\rho_{GERG\text{-}improved}$.

T/K[a]	p/MPa[a]	ρ_{exp}/(kg·m^{-3})[(a)]	U (ρ_{exp})/(kg·m^{-3})	10^2 U (ρ_{exp})/ρ_{exp}	10^2 (ρ_{exp} − $\rho_{AGA8\text{-}DC92}$)/$\rho_{AGA8\text{-}DC92}$	10^2 (ρ_{exp} − $\rho_{GERG\text{-}2008}$)/$\rho_{GERG\text{-}2008}$	10^2 (ρ_{exp} − $\rho_{GERG\text{-}improved}$)/$\rho_{GERG\text{-}improved}$
250.000 K							
250.134	19.85938	160.136	0.041	0.026	−0.119	−0.108	−0.123
250.133	19.05712	154.693	0.040	0.026	−0.089	−0.099	−0.146
250.134	18.06430	147.637	0.040	0.027	−0.053	−0.085	−0.167
250.132	17.03403	139.940	0.039	0.028	−0.019	−0.070	−0.181
250.132	16.04267	132.179	0.038	0.029	0.008	−0.054	−0.186
250.130	15.04385	124.038	0.037	0.030	0.035	−0.032	−0.179
250.131	14.03791	115.535	0.036	0.031	0.056	−0.011	−0.167
250.133	13.03272	106.796	0.035	0.033	0.077	0.018	−0.144
250.132	12.03336	97.915	0.034	0.035	0.080	0.035	−0.131
250.135	11.02191	88.824	0.033	0.037	0.085	0.060	−0.111
250.133	10.02295	79.806	0.032	0.040	0.071	0.070	−0.106
250.133	9.01852	70.792	0.031	0.044	0.056	0.080	−0.100
250.133	8.01228	61.881	0.030	0.048	0.030	0.078	−0.102
250.131	7.01013	53.193	0.029	0.054	0.007	0.074	−0.101
250.131	6.00760	44.730	0.028	0.063	−0.021	0.059	−0.104
250.132	5.00600	36.542	0.027	0.074	−0.046	0.040	−0.106
250.133	4.00423	28.641	0.026	0.091	−0.060	0.022	−0.101
250.149	3.00373	21.046	0.025	0.120	−0.063	0.008	−0.087
250.147	2.00285	13.751	0.024	0.178	−0.029	0.025	−0.040
250.147	1.00235	6.747	0.024	0.350	0.066	0.096	0.063
275.000 K							
275.111	19.79474	135.100	0.038	0.028	−0.057	−0.053	−0.114
275.105	18.04682	124.117	0.037	0.030	−0.043	−0.049	−0.107
275.105	17.04594	117.552	0.036	0.031	−0.034	−0.044	−0.099
275.104	16.03762	110.752	0.035	0.032	−0.028	−0.042	−0.092
275.104	15.03508	103.826	0.035	0.033	−0.023	−0.039	−0.086
275.102	14.03092	96.750	0.034	0.035	−0.021	−0.037	−0.083
275.085	13.02770	89.570	0.033	0.037	−0.030	−0.043	−0.091
275.094	12.02608	82.322	0.032	0.039	−0.026	−0.034	−0.087
275.098	11.01666	74.976	0.031	0.042	−0.022	−0.024	−0.082
275.100	10.01570	67.674	0.031	0.045	−0.031	−0.025	−0.090
275.097	9.01262	60.383	0.030	0.049	−0.042	−0.027	−0.099
275.096	8.01109	53.160	0.029	0.054	−0.053	−0.029	−0.106
275.096	7.00908	46.020	0.028	0.061	−0.059	−0.029	−0.107
275.098	6.00648	38.986	0.027	0.070	−0.064	−0.029	−0.104
275.098	5.00590	32.097	0.027	0.083	−0.067	−0.029	−0.098
275.089	4.00439	25.349	0.026	0.102	−0.065	−0.028	−0.089
275.098	3.00345	18.761	0.025	0.133	−0.056	−0.022	−0.070
275.097	2.00254	12.341	0.024	0.197	−0.029	−0.003	−0.036
275.094	1.00209	6.093	0.024	0.387	0.026	0.042	0.024
300.000 K							
300.065	19.88020	118.054	0.036	0.031	−0.030	−0.024	−0.034
300.062	19.02143	113.328	0.036	0.032	−0.029	−0.024	−0.028
300.064	18.02455	107.722	0.035	0.033	−0.026	−0.022	−0.020
300.065	17.01538	101.923	0.034	0.034	−0.024	−0.022	−0.014
300.064	16.01979	96.095	0.034	0.035	−0.022	−0.022	−0.011
300.065	15.01664	90.124	0.033	0.037	−0.019	−0.020	−0.008
300.065	14.01926	84.105	0.032	0.039	−0.017	−0.020	−0.009
300.065	13.01358	77.969	0.032	0.041	−0.016	−0.019	−0.012
300.064	12.01564	71.830	0.031	0.043	−0.016	−0.018	−0.016
300.062	11.01460	65.644	0.030	0.046	−0.010	−0.010	−0.016
300.061	10.00901	59.408	0.030	0.050	−0.015	−0.013	−0.025
300.060	9.01290	53.239	0.029	0.054	−0.013	−0.008	−0.027
300.061	8.00924	47.042	0.028	0.060	−0.015	−0.007	−0.031
300.059	7.00775	40.898	0.028	0.067	−0.014	−0.003	−0.031
300.062	6.00537	34.800	0.027	0.077	−0.014	<0.001	−0.029
300.061	5.00462	28.778	0.026	0.091	−0.014	0.002	−0.026
300.061	4.00319	22.830	0.025	0.112	−0.013	0.003	−0.021
300.062	3.00277	16.975	0.025	0.146	−0.012	0.004	−0.017
300.062	2.00253	11.219	0.024	0.215	0.007	0.020	0.006
300.063	1.00253	5.564	0.023	0.422	0.033	0.042	0.034
325.000 K							
325.068	19.91762	105.164	0.035	0.033	−0.029	−0.022	0.004
325.070	19.03166	100.796	0.034	0.034	−0.030	−0.023	0.008
325.072	18.02626	95.755	0.034	0.035	−0.032	−0.026	0.010
325.075	17.02502	90.653	0.033	0.037	−0.031	−0.027	0.012
325.074	16.02207	85.467	0.033	0.038	−0.031	−0.028	0.012
325.078	15.01620	80.196	0.032	0.040	−0.030	−0.028	0.010
325.080	14.01608	74.897	0.031	0.042	−0.028	−0.028	0.008
325.081	13.01381	69.537	0.031	0.044	−0.027	−0.028	0.004

(*continued on next page*)

Table 6 (*continued*)

T/K[a]	p/MPa[a]	ρ_{exp}/(kg·m^{-3})[(a)]	$U(\rho_{exp})$/(kg·m^{-3})	$10^2\,U(\rho_{exp})/\rho_{exp}$	$10^2(\rho_{exp}-\rho_{AGA8\text{-}DC92})/\rho_{AGA8\text{-}DC92}$	$10^2(\rho_{exp}-\rho_{GERG\text{-}2008})/\rho_{GERG\text{-}2008}$	$10^2(\rho_{exp}-\rho_{GERG\text{-}improved})/\rho_{GERG\text{-}improved}$
325.081	12.01465	64.153	0.030	0.047	−0.026	−0.028	−0.001
325.080	11.01158	58.724	0.030	0.050	−0.018	−0.021	0.001
325.080	10.00777	53.265	0.029	0.054	−0.020	−0.022	−0.007
325.083	9.01024	47.834	0.028	0.059	−0.017	−0.019	−0.009
325.080	8.00638	42.370	0.028	0.065	−0.021	−0.021	−0.016
325.076	7.00438	36.931	0.027	0.073	−0.019	−0.017	−0.016
325.076	6.00516	31.529	0.026	0.084	−0.021	−0.017	−0.019
325.078	5.00390	26.146	0.026	0.099	−0.024	−0.018	−0.022
325.077	4.00361	20.810	0.025	0.121	−0.026	−0.020	−0.023
325.081	3.00304	15.519	0.025	0.159	−0.035	−0.027	−0.031
325.076	2.00278	10.288	0.024	0.234	−0.036	−0.028	−0.031
325.078	1.00254	5.117	0.023	0.458	−0.035	−0.029	−0.031
350.000 K							
350.086	19.91259	95.026	0.034	0.035	−0.030	−0.025	0.017
350.083	19.01409	91.018	0.033	0.037	−0.032	−0.027	0.019
350.088	18.01116	86.481	0.033	0.038	−0.030	−0.026	0.022
350.089	17.01022	81.891	0.032	0.039	−0.030	−0.027	0.023
350.090	16.00870	77.239	0.032	0.041	−0.028	−0.027	0.023
350.091	15.01019	72.551	0.031	0.043	−0.025	−0.025	0.024
350.092	14.00745	67.794	0.031	0.045	−0.023	−0.025	0.022
350.093	13.00789	63.011	0.030	0.048	−0.021	−0.024	0.019
350.091	12.00843	58.193	0.029	0.051	−0.019	−0.023	0.016
350.092	11.00574	53.335	0.029	0.054	−0.011	−0.015	0.019
350.092	10.00748	48.471	0.028	0.059	−0.011	−0.015	0.015
350.091	9.00560	43.576	0.028	0.064	−0.012	−0.015	0.010
350.095	8.00468	38.677	0.027	0.071	−0.010	−0.012	0.009
350.096	7.00500	33.785	0.027	0.079	−0.008	−0.009	0.008
350.094	6.00374	28.888	0.026	0.091	−0.012	−0.012	0.003
350.094	5.00298	24.006	0.026	0.107	−0.018	−0.016	−0.004
350.093	4.00375	19.151	0.025	0.131	−0.024	−0.020	−0.011
350.092	3.00275	14.311	0.024	0.171	−0.038	−0.032	−0.025
350.094	2.00271	9.507	0.024	0.252	−0.051	−0.045	−0.040
350.094	1.00247	4.739	0.023	0.494	−0.057	−0.051	−0.049

[a] Expanded uncertainties ($k = 2$): $U(p > 3)/\text{MPa} = 75{\cdot}10^{-6}.\frac{p}{\text{MPa}} + 3.5{\cdot}10^{-3}$; $U(p < 3)/\text{MPa} = 60{\cdot}10^{-6}.\frac{p}{\text{MPa}} + 1.7{\cdot}10^{-3}$; $U(T) = 15$ mK; $\frac{U(\rho)}{\text{kg·m}^{-3}} = 2.5{\cdot}10^{4}\frac{\chi_S}{\text{m}^3\text{kg}^{-1}} + 1.1{\cdot}10^{-4}.\frac{\rho}{\text{kg·m}^{-3}} + 2.3{\cdot}10^{-2}$.

4. Discussion

4.1. Relative deviations of experimental data from the reference equations of state

Percentage relative deviations of experimental density data from the density calculated with the mixture models of AGA8-DC92 EoS, GERG-2008 EoS, and improved-GERG-2008 EoS are depicted in Figs. 2–4, for the G 431, G 453, and G 454 mixtures, respectively.

Table 7 reports a statistical comparison of the experimental density data obtained in this work and other literature data dealing with H_2-enriched multicomponent mixtures [27,50] with respect to AGA8-DC92 EoS, GERG-2008 EoS, and improved-GERG-2008 EoS. Here, *AARD* stands for the average absolute relative deviations, *BiasRD* the average relative deviation, *RMSRD* the root mean square relative deviation, and *MaxRD* maximum relative deviation, as expressed in Eqs. (4)–(7):

$$AARD = \frac{1}{N}\sum_{i=1}^{N}\left|10^2\frac{\rho_{i,exp}-\rho_{i,EoS}}{\rho_{i,EoS}}\right| \quad (4)$$

$$BiasRD = \frac{1}{N}\sum_{i=1}^{N}\left(10^2\frac{\rho_{i,exp}-\rho_{i,EoS}}{\rho_{i,EoS}}\right) \quad (5)$$

$$RMSRD = \sqrt{\frac{1}{N}\sum_{i=1}^{N}\left(10^2\frac{\rho_{i,exp}-\rho_{i,EoS}}{\rho_{i,EoS}}\right)^2} \quad (6)$$

$$MaxRD = \max\left|10^2\frac{\rho_{i,exp}-\rho_{i,EoS}}{\rho_{i,EoS}}\right| \quad (7)$$

Fig. 2 shows that relative deviations between experimental density data for the H_2-free natural gas mixture (G 431) and any of the three EoS used for comparison are always smaller than the claimed uncertainties of the EoS ($U(\rho_{EoS}) = 0.1$ %). The three EoS applied to our results represent the experimental density data very well, with maximum relative deviations around 0.05 % and AARD between 0.012 % when comparing to AGA8-DC92 and 0.032 % with respect to the GERG-2008 EoS.

Regarding the G 453 H_2-enriched natural gas mixture (G 431 + 10 % H_2), the relative deviations from the EoS, as shown in Fig. 3, are larger than the EoS uncertainty, $U(\rho_{EoS})$, stated by the EoS only for the lowest isotherm of 250 K and pressures above 16 MPa when comparing to the AGA8-DC92 EoS; above 13 MPa when comparing to GERG-2008 EoS; and only above a pressure as low as 4 MPa when comparing to the improved-GERG-2008 EoS. Maximum relative deviations of near 0.20 % can be seen with respect to any of the three EoS for the lowest temperature. The average absolute value of the relative deviation of the experimental density data with respect to the AGA8-DC92 and GERG-2008 EoS is around 0.030 %. A slightly worse agreement, however, is obtained with respect to the improved GERG-2008 EoS, with an AARD of 0.047 %. A similar behavior could be observed in the density of a binary mixture composed of methane and hydrogen (0.90 CH_4 + 0.10 H_2), performed with this same experimental technique and published in a previous work [51].

Fig. 4 shows that the relative deviations of the experimental density data for the G 454 H_2-enriched natural gas mixture (G 431 + 20 % H_2), with respect to the AGA8-DC92 and the GERG-2008 EoS, are always smaller than the stated uncertainty of the EoS, except for one single point at the lowest temperature ($T = 250$ K) and the highest pressure (p

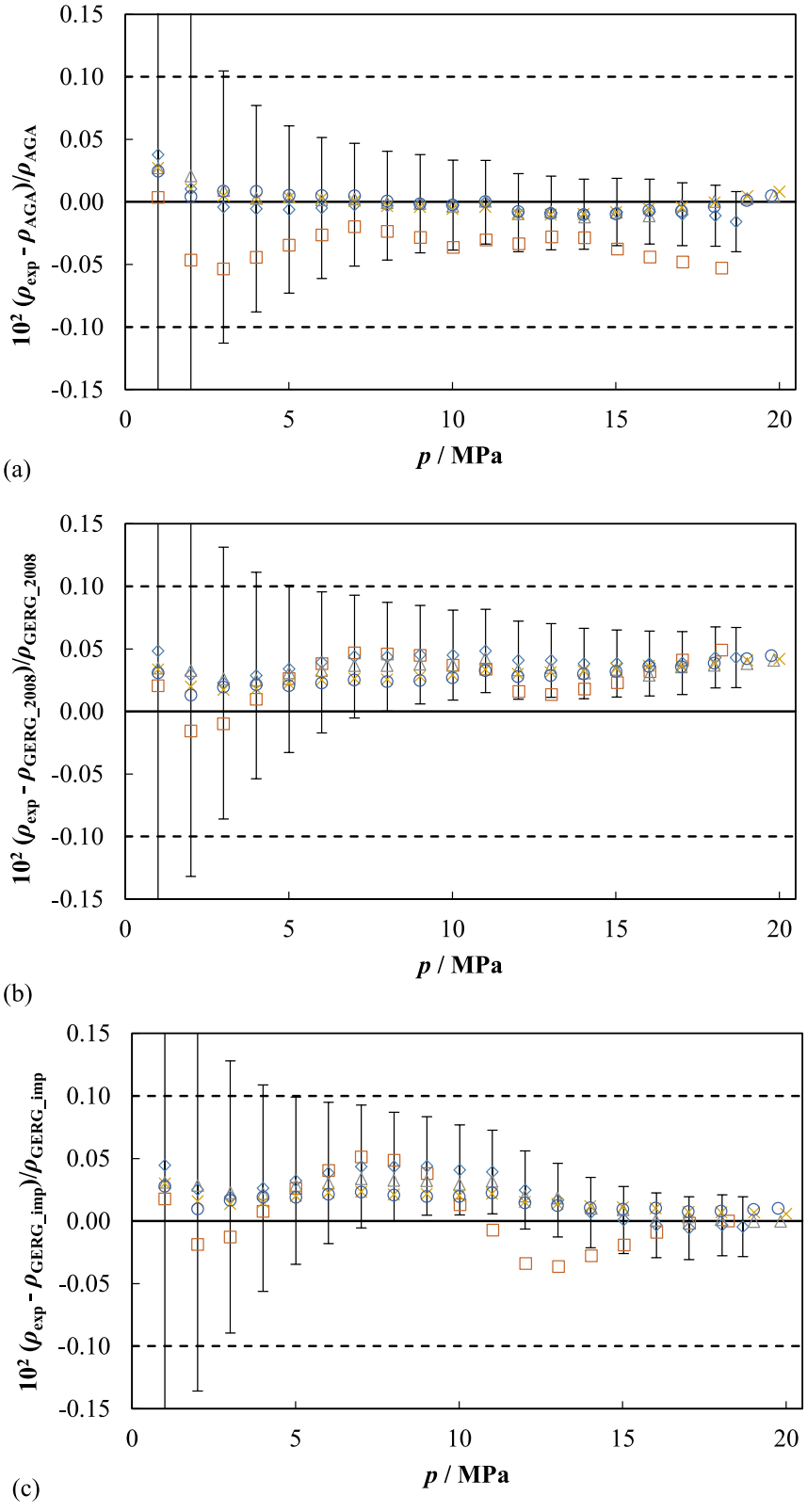

Fig. 2. Relative deviations in density of experimental (p, ρ_{exp}, T) data of the (H_2-free) natural gas mixture G 431 from density values calculated from (a) AGA8-DC92 EoS [19], $\rho_{AGA8\text{-}DC92}$, (b) GERG-2008 EoS [20,21], $\rho_{GERG\text{-}2008}$, and (c) improved-GERG-2008 EoS [44–46], $\rho_{GERG\text{-}improved}$, as a function of the pressure for different temperatures: □ 250 K, ◇ 275 K, △ 300 K, × 325 K, ○ 350 K. Dashed lines indicate the expanded ($k = 2$) uncertainty of the corresponding EoS. Error bars on the 275-K data set indicate the expanded ($k = 2$) uncertainty of the experimental density.

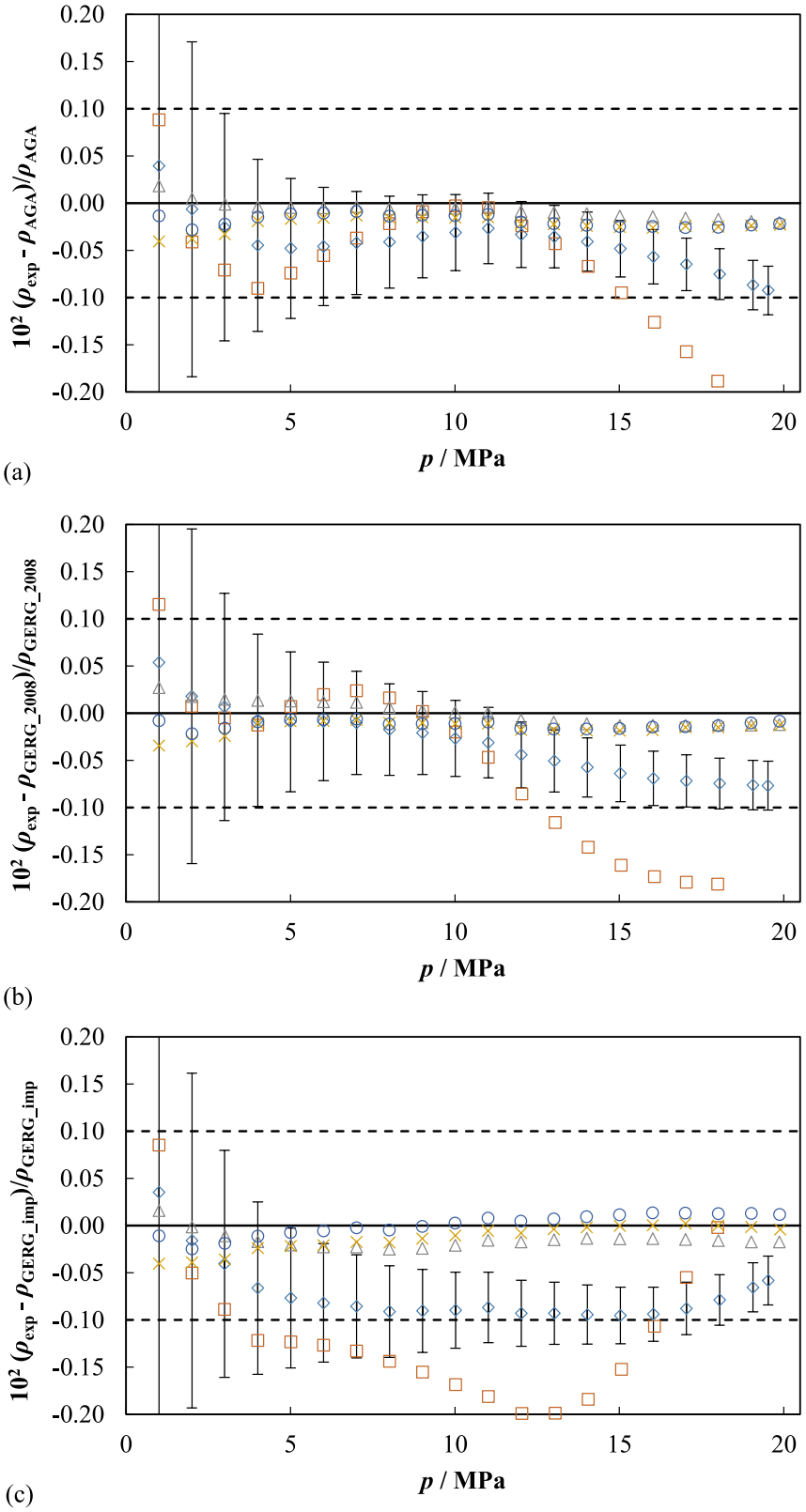

Fig. 3. Relative deviations in density of experimental (p, ρ_{exp}, T) data of the (H_2-enriched) natural gas mixture G 453 (G 431 + 10 % H_2) from density values calculated from (a) AGA8-DC92 EoS [19], $\rho_{AGA8\text{-}DC92}$, (b) GERG-2008 EoS [20,21], $\rho_{GERG\text{-}2008}$, and (c) improved-GERG-2008 EoS [44–46], $\rho_{GERG\text{-}improved}$, as a function of the pressure for different temperatures: □ 250 K, ◇ 275 K, △ 300 K, × 325 K, ○ 350 K. Dashed lines indicate the expanded (k = 2) uncertainty of the corresponding EoS. Error bars on the 275-K data set indicate the expanded (k = 2) uncertainty of the experimental density.

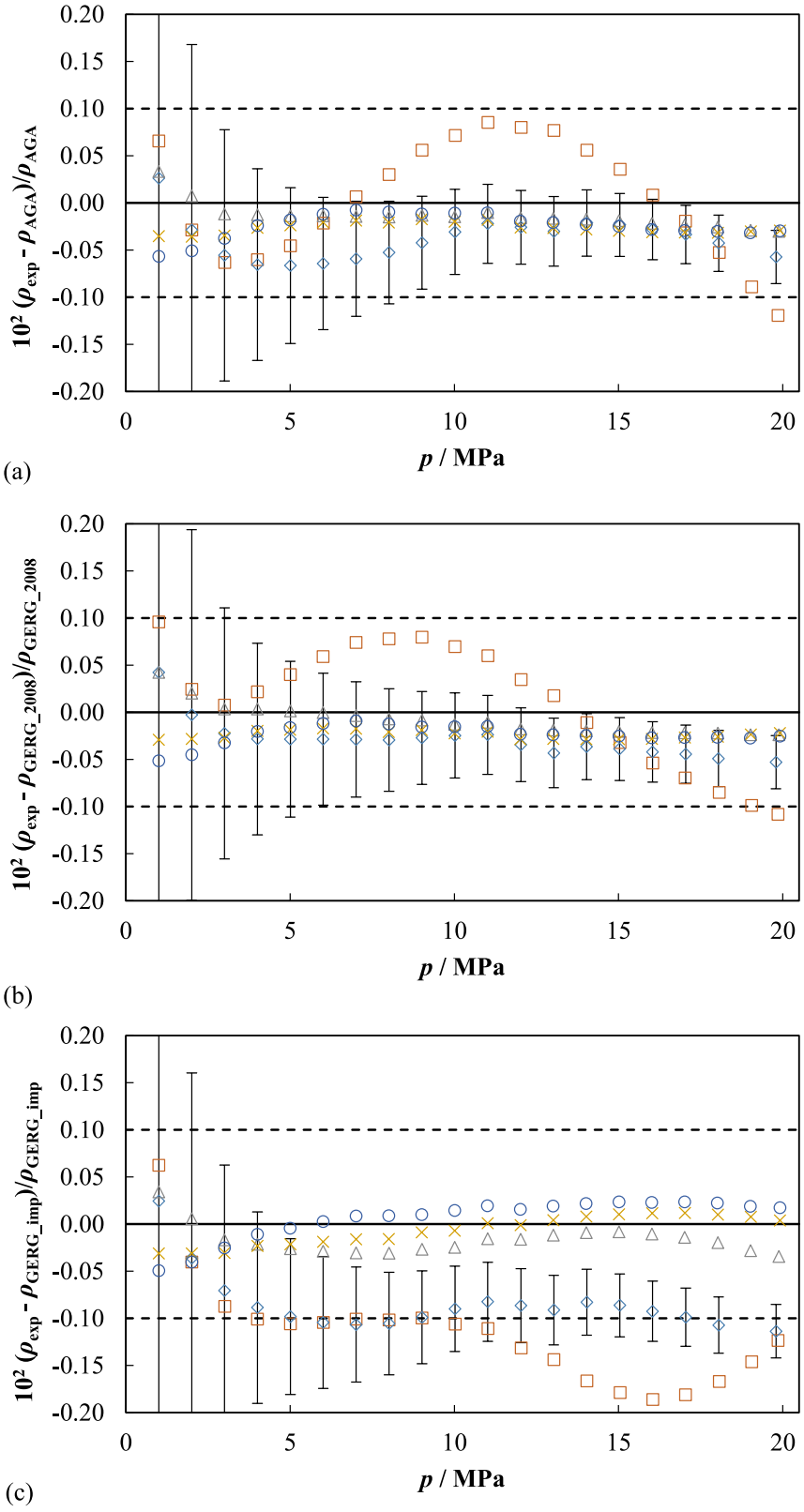

Fig. 4. Relative deviations in density of experimental (p, ρ_{exp}, T) data of the (H_2-enriched) natural gas mixture G 454 (G 431 + 20 % H_2) from density values calculated from (a) AGA8-DC92 EoS [19], $\rho_{AGA8\text{-}DC92}$, (b) GERG-2008 EoS [20,21], $\rho_{GERG\text{-}2008}$, and (c) improved-GERG-2008 EoS [44–46], $\rho_{GERG\text{-}improved}$, as a function of the pressure for different temperatures: □ 250 K, ◇ 275 K, △ 300 K, × 325 K, ○ 350 K. Dashed lines indicate the expanded (k = 2) uncertainty of the corresponding EoS. Error bars on the 275-K data set indicate the expanded (k = 2) uncertainty of the experimental density.

Table 7
Statistical analysis of the (p, ρ, T) data sets with respect to AGA8-DC92 EoS [19], GERG-2008 EoS [20,21], and improved-GERG-2008 EoS [44–46] for all the natural gas mixtures studied in this work, including literature data for comparable mixtures. *AARD* = average absolute value of the relative deviations, *BiasRD* = average relative deviation, *RMSRD* = root mean square relative deviation, *MaxRD* = maximum value of the relative deviations.

Reference[a]	x_{H_2}	n[b]	Covered ranges		Experimental vs AGA8-DC92 EoS				Experimental vs GERG-2008 EoS				Experimental vs improved-GERG-2008 EoS			
			T/K	p/MPa	*AARD*/%	*BiasRD*/%	*RMSRD*/%	*MaxRD*/%	*AARD*/%	*BiasRD*/%	*RMSRD*/%	*MaxRD*/%	*AARD*/%	*BiasRD*/%	*RMSRD*/%	*MaxRD*/%
G 431 (this work)	0	97	250–350	1–20	0.012	−0.0066	0.018	0.054	0.032	0.032	0.034	0.049	0.019	0.016	0.023	0.051
G 453 (this work)	0.099928	98	275–350	1–20	0.032	−0.029	0.045	0.19	0.029	−0.021	0.049	0.18	0.047	−0.042	0.070	0.20
G 454 (this work)	0.199945	99	250–350	1–20	0.033	−0.020	0.039	0.12	0.030	−0.015	0.037	0.11	0.052	−0.043	0.072	0.19
Hernández-Gómez et al., 2018 [27]	0.030097	99	260–350	1–20	0.066	−0.066	0.074	0.20	0.10	−0.10	0.13	0.31	0.13	−0.12	0.15	0.33
Richter et al., 2014 [50] [c]	0.053681	37	273–293	1–8	0.059	−0.059	0.061	0.078	0.041	−0.041	0.044	0.075	0.094	−0.094	0.10	0.14
Richter et al., 2014 [50] [c]	0.104106	36	273–293	1–8	0.019	−0.010	0.021	0.039	0.021	0.019	0.026	0.055	0.054	−0.054	0.061	0.10
Richter et al., 2014 [50] [c]	0.304705	13	283	1–8	0.26	−0.26	0.26	0.27	0.21	−0.21	0.21	0.27	0.26	−0.26	0.27	0.32

[a] Only vapor and supercritical phase measurements have been considered.
[b] Number of experimental points.
[c] Only experimental mass densities were considered.

= 20 MPa). The *AARD* value from these two EoS is around 0.030 %, similar to the value obtained for the natural gas mixture with 10 % of hydrogen (G 453). Again, a slightly worse agreement is obtained with the improved GERG-2008 EoS, with a maximum relative deviation of 0.19 % and an *AARD* of 0.052 %. Surprisingly, when comparing the experimental density data to the improved GERG-2008 EoS, not only some points at the lowest temperature ($T = 250$ K) and highest pressures ($p > 10$ MPa) have deviations larger than the stated uncertainty of the EoS, but also some points at $T = 275$ K.

It can be observed that the relative deviations at the lowest pressures for the H_2-free natural gas mixture (G 431) do not exactly tend to zero, as would be expected for approximating an ideal gas behavior; while for the two H_2-enriched natural gas mixtures (G 453 and G 454), there is additionally a pronounced dispersion, that is, a wider range of deviation for different temperatures, in the low-pressure data ($p = 1$ MPa). Sorption phenomena, which can slightly change the composition of the mixture and thus alter the density measurements, mainly in complex mixtures with numerous components as the three mixtures studied here, may be related with the deviation and dispersion of the lowest pressure data. The influence of adsorption and desorption on accurate density measurement of multicomponent gas mixtures was investigated in depth by Richter and Kleinrahm in Ref. [52]. The applied measurement procedure aims to minimize these sorption phenomena by evacuating and filling the cell several times and repeating some selected points within the challenging p, T region over long periods of time, but in the experimental technique used in this work, the single-sinker densimeter is not appropriate to quantify this effect. In any case, we consider these deviations well below the uncertainty of the experimental data, which at lower pressures and densities is relatively high.

In general, we could prove that the AGA8-DC92 EoS is the model that performs best for the H_2-free sample (*AARD* = 0.012 %), while GERG-2008 EoS is slightly better at predicting the densities for the two investigated H_2-enriched mixtures (*AARD* = 0.030 %), although the differences between these two equations are not significant. In contrast, the improved-GERG-2008 EoS reproduces the data with larger deviations in comparison to the other two reference models for the three mixtures, with *AARD* values as high as 0.052 % and *MaxRD* about 0.20 % for the samples containing hydrogen. In multiparametric Helmholtz models, the fitting of a single property affects the description of the other properties, with an accuracy strongly dependent on the amount and quality of the experimental data used for the adjustment. Thus, it seems that the corrections made in the improved GERG-2008 EoS to cover the subcooled temperature range of LNG applications and to correct unphysical phase envelopes of binary mixtures with hydrogen for isotherms below 120 K have shifted the density estimations for some of the points at supercritical pipeline conditions to slightly worse values than those obtained by the original GERG-2008 EoS.

In a previous study, Hernández-Gómez et al. [27] determined densities for a 3 % H_2-natural gas mixture, using the same single-sinker with magnetic coupling employed here. The measurements were carried out in temperature and pressure ranges similar to the ones explored here, namely between (260–350) K and up to 20 MPa, estimating an experimental expanded ($k = 2$) uncertainty ranging from (0.029–0.50) %. They found relative deviations that rise to 0.19 % as compared to predictions from AGA8-DC92 EoS, and to 0.29 % according to estimations from GERG-2008 EoS, at the lowest isotherm of 260 K and pressures higher than 15 MPa. Though these discrepancies are of the same order of magnitude as the ones obtained for the G 453 mixture (G 431 + 10 % H_2) at similar conditions, we assume that they could be caused not only by the relatively small addition of 3 % H_2, but by the significant amounts of CO_2 (4 mol-%) and N_2 (12 mol-%), as well as the higher concentrations of ethane, propane, and butane of that mixture. These differences could be partly explained by the deviations found for the binary mixtures of ($CH_4 + CO_2$) [53] and ($CH_4 + N_2$) [41].

Richter et al. [50] studied the density of a pipeline natural gas blended with hydrogen at three different concentrations of (0.05, 10,

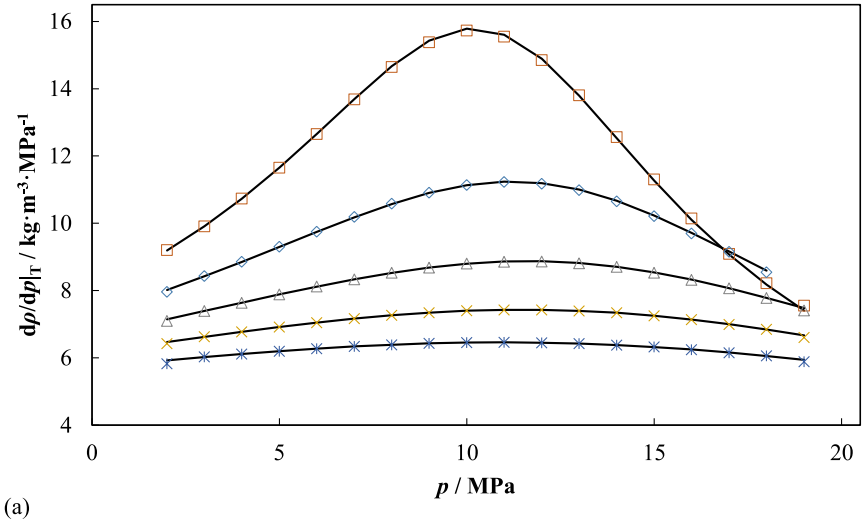

(a)

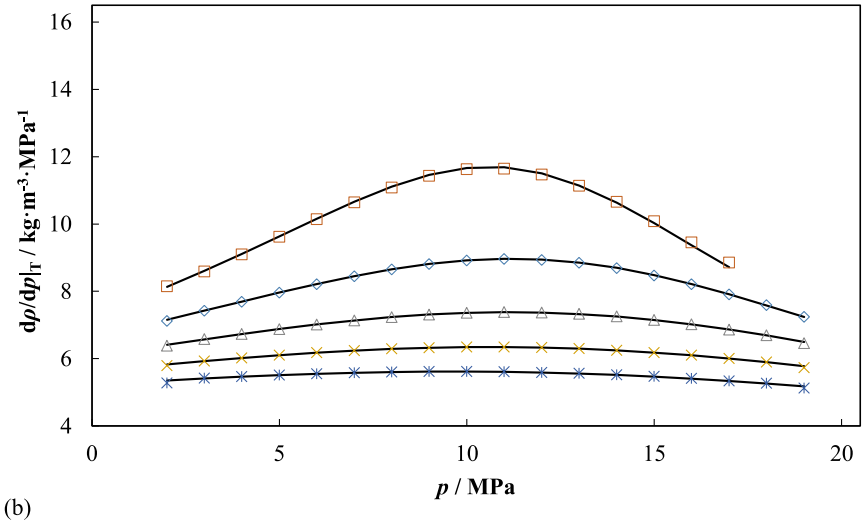

(b)

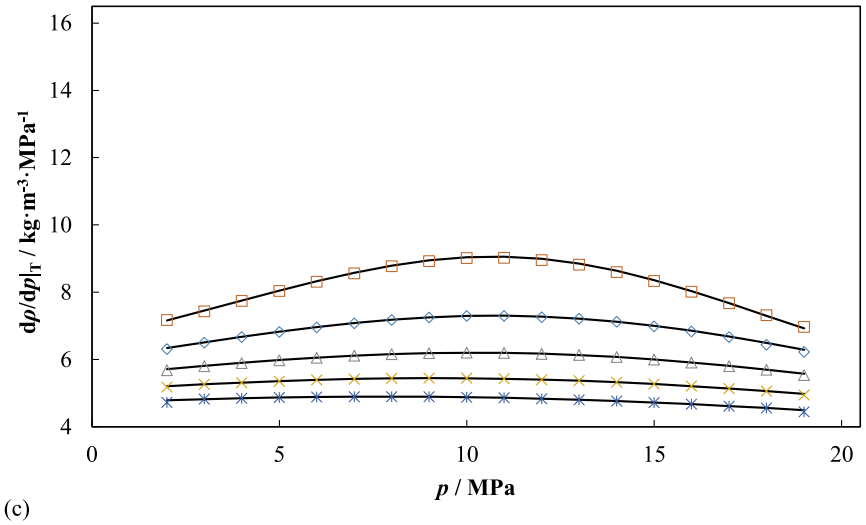

(c)

Fig. 5. Derived $\left.\frac{\partial \rho_{exp}}{\partial p}\right|_T$ values of (a) G 431, (b) G 453 (G 431 + 10 % H_2), and (c) G 454 (G 431 + 20 % H_2) mixtures as a function of the pressure for different temperatures: □ 250 K, ◇ 275 K, △ 300 K, × 325 K, ○ 350 K. Solid lines indicate the $\left.\frac{\partial \rho_{EoS}}{\partial p}\right|_T$ values calculated from the improved-GERG-2008 EoS [44–46].

Table 8
Derived isothermal compressibility κ_T values for all the reference natural gas mixtures studied in this work at various temperatures T and pressures p.

κ_T/MPa^{-1} [a]					
	T/K				
p/MPa	250	275	300	325	350
G 431					
19	0.0335		0.0480	0.0495	0.0497
18	0.0378	0.0486	0.0530	0.0540	0.0539
17	0.0435	0.0548	0.0581	0.0583	0.0579
16	0.0509	0.0615	0.0636	0.0632	0.0625
15	0.0599	0.0692	0.0698	0.0686	0.0675
14	0.0711	0.0776	0.0766	0.0746	0.0730
13	0.0844	0.0869	0.0840	0.0813	0.0793
12	0.0995	0.0970	0.0923	0.0889	0.0865
11	0.1160	0.1079	0.1016	0.0976	0.0949
10	0.1329	0.1199	0.1123	0.1077	0.1048
9	0.1497	0.1333	0.1247	0.1197	0.1165
8	0.1670	0.1489	0.1397	0.1345	0.1311
7	0.1861	0.1678	0.1585	0.1531	0.1495
6	0.2097	0.1923	0.1830	0.1775	0.1739
5	0.2418	0.2258	0.2169	0.2114	0.2077
4	0.2900	0.2757	0.2672	0.2618	0.2580
3	0.3711	0.3590	0.3509	0.3457	0.3423
2	0.5361	0.5215	0.5142	0.5088	0.5001
G 453 (G 431 + 10 % H_2)					
19		0.0468	0.0488	0.0494	0.0493
18		0.0515	0.0533	0.0535	0.0534
17	0.0519	0.0567	0.0577	0.0575	0.0571
16	0.0585	0.0624	0.0627	0.0621	0.0614
15	0.0664	0.0688	0.0682	0.0671	0.0662
14	0.0754	0.0758	0.0743	0.0727	0.0716
13	0.0854	0.0836	0.0811	0.0791	0.0777
12	0.0963	0.0922	0.0887	0.0863	0.0846
11	0.1082	0.1019	0.0976	0.0947	0.0928
10	0.1212	0.1129	0.1078	0.1047	0.1026
9	0.1354	0.1256	0.1200	0.1165	0.1142
8	0.1516	0.1408	0.1348	0.1311	0.1286
7	0.1710	0.1598	0.1535	0.1496	0.1470
6	0.1956	0.1845	0.1781	0.1741	0.1713
5	0.2292	0.2184	0.2120	0.2079	0.2051
4	0.2789	0.2686	0.2624	0.2585	0.2554
3	0.3614	0.3522	0.3463	0.3424	0.3397
2	0.5286	0.5165	0.5106	0.5064	0.4989
G 454 (G 431 + 20 % H_2)					
19	0.0452	0.0479	0.0489	0.0491	0.0489
18	0.0497	0.0520	0.0529	0.0529	0.0527
17	0.0549	0.0568	0.0570	0.0567	0.0564
16	0.0608	0.0618	0.0616	0.0610	0.0605
15	0.0673	0.0674	0.0666	0.0658	0.0651
14	0.0746	0.0737	0.0723	0.0712	0.0703
13	0.0827	0.0806	0.0787	0.0773	0.0763
12	0.0917	0.0884	0.0860	0.0843	0.0831
11	0.1018	0.0974	0.0945	0.0925	0.0912
10	0.1132	0.1079	0.1045	0.1023	0.1008
9	0.1263	0.1202	0.1164	0.1140	0.1123
8	0.1419	0.1352	0.1310	0.1285	0.1266
7	0.1611	0.1540	0.1496	0.1468	0.1449
6	0.1860	0.1786	0.1741	0.1712	0.1692
5	0.2200	0.2126	0.2080	0.2050	0.2029
4	0.2703	0.2631	0.2585	0.2555	0.2532
3	0.3533	0.3470	0.3424	0.3394	0.3374
2	0.5215	0.5121	0.5073	0.5040	0.4975

[a] Expanded ($k = 2$) uncertainty: U_r (κ_T) = 0.7 %.

and 30) mol-%. The characterization was performed with a two-sinker magnetic suspension densimeter in a narrow temperature range of (273.15, 283.15, and 293.15) K and up to a pressure of 8 MPa. They estimated a low experimental expanded ($k = 2$) uncertainty of only 0.02 % for densities larger than 3 kg m^{-3}. Note that the data for the mixture with 30 % of H_2 in the work of Richter et al. are reported in Table 7 just for completeness but not considered in the discussion of our work because, first, the density is only determined for one isotherm, 283.15 K, and second, the results show a negative deviation of 0.26 %, independently of the pressure. The authors of that work attributed this issue to the technical impossibility of a correct analysis of the mixture composition. It is tackled by fitting the mass density results to a second order virial expansion, from which an average experimental molar mass is determined, differing from the one given by the analyzed gas composition. Then, adjusted results are obtained in terms of shifted molar densities, which are calculated using the experimental value for the molar mass and the original data sets. Notably, in the limited pressure range of 8 MPa and intermediate isotherms explored by Richter et al. [50], there is a good agreement between our data for the G 453 mixture (G 431 + 10 % H_2) and the results of their work for the 10 % H_2 mixture. Both works show relative deviations of experimental data increasing as the temperature decreases, but only within a 0.05 % band, and a nearly constant discrepancy with temperature between AGA8-DC92 EoS and GERG-2008 EoS of about 0.04 %, which cancels out for pressures around 8 MPa. The differences between their work and ours are that we see negative deviations and a better performance of the GERG-2008 EoS model; while in their case, all deviations are positive and the AGA8-DC92 EoS reproduces their data in a better way. We assume this is again related to the difference in the composition between the studied mixtures, the 10 % H_2 mixture of Richter et al. has a lower CH_4 content, but a concentration of CO_2 five times higher and significant amounts of C_2H_6 and C_3H_8, apart from traces of heavier hydrocarbons (C_{7+}).

4.2. Isothermal compressibility

From the values of the experimental density, further information can be obtained from its derivatives. Fig. 5 illustrates the partial derivatives of experimental density as a function of pressure, $\left.\frac{\partial \rho_{exp}}{\partial p}\right|_T$, and Table 8 lists the corresponding isothermal compressibility values, $\kappa_T = \frac{1}{\rho_{exp}} \left.\frac{\partial \rho_{exp}}{\partial p}\right|_T$, for the three studied mixtures in this work. They were obtained by a cubic spline interpolation of the measured density data sets; for this reason, the values at maximum and minimum pressure of each isotherm were not considered and consequently discarded. These partial derivatives show an increasingly convex shape as the temperature decreases, which flattens with increasing hydrogen content for the range of pressures and temperatures studied. The κ_T values range from (0.0335–0.5361) MPa^{-1} at 250 K for the H_2-free natural gas mixture, decreasing when both the temperature and hydrogen concentration increase.

As can be seen from the solid lines in Fig. 5, there is a good agreement with the predicted $\left.\frac{\partial \rho_{EoS}}{\partial p}\right|_T$ from the improved-GERG-2008 EoS, and the relative deviations of experimental κ_T from predicted values from the improved-GERG-2008 EoS result in *AARD* of (0.18, 0.14, and 0.13) % and *MaxRD* of (2.0, 1.7, and 1.3) % for the H_2-free (G 431), 10 % H_2 (G 453), and 20 % H_2 (G 454) mixtures, respectively. In all cases, they are within the estimated experimental expanded ($k = 2$) uncertainty of κ_T, U_r (κ_T) = 0.7 %.

5. Conclusions

The performance of the reference equations of state commonly used for natural gas when applied to H2NG mixtures should be checked before its generalized use for process design and custody transfer applications. For this purpose, density measurements of three synthetic natural gas related mixtures from (250–350) K and pressures up to 20 MPa were performed using a high-accuracy single-sinker magnetic suspension densimeter. The first mixture is an 11-compound mixture representative of a typical high-calorific natural gas composed mainly of methane (>97 %). The following two mixtures were elaborated by the addition of hydrogen to the first one until a nominal composition of (10 and 20) mol-%, respectively, is reached. The three mixtures were prepared gravimetrically in order to achieve the maximum possible accuracy in their composition.

The experimental density results were compared to the densities given by three different reference equations of state for natural gas related mixtures: the AGA8-DC92 EoS, the GERG-2008 EoS, and an improved version of the GERG-2008 EoS. In general, while relative deviations of the experimental density data for the hydrogen-free natural gas mixture are always within the claimed uncertainty of the three considered equations of state, larger deviations can be observed for the H2NG mixtures from any of the three equations of state, especially for the lowest temperature and the highest pressures, with maximum relative deviations of near 0.20 % with respect to any of the three EoS, above their claimed uncertainty of 0.1 %.

The conclusions obtained from this study are only valid for natural gas mixtures composed mainly of methane when hydrogen is added up to 20 %. More research is needed to evaluate the performance of these reference EoS for H2NG mixtures when the starting natural gas to which hydrogen is added has a different composition and/or the hydrogen added gives a concentration above 20 mol-%. The study of H2NG mixtures with up to 20 mol-% of hydrogen obtained by injecting hydrogen to natural gas mixtures with significant amounts of ethane, propane, butane, nitrogen, or carbon dioxide are of special interest.

CRediT authorship contribution statement

Daniel Lozano-Martín: Data curation, Formal analysis, Investigation, Software, Writing – original draft, Visualization. **Fatemeh Pazoki:** Data curation, Investigation. **Heinrich Kipphardt:** Data curation, Investigation. **Peyman Khanipour:** Data curation, Investigation. **Dirk Tuma:** Conceptualization, Investigation, Project administration, Writing – review & editing. **Alfonso Horrillo:** Data curation, Investigation. **César R. Chamorro:** Conceptualization, Funding acquisition, Investigation, Project administration, Supervision, Writing – review & editing.

Declaration of competing interest

The authors declare that they have no known competing financial interests or personal relationships that could have appeared to influence the work reported in this paper.

Acknowledgments

This work was funded by the European Metrology Programme on Innovation and Research (EMPIR), Funder ID: 10.13039/100014132, Grant No. 19ENG03 MefHySto, and by the Regional Government of Castilla y León (Junta de Castilla y León), the Ministry of Science and Innovation MCIN, and the European Union NextGenerationEU/PRTR, project C17.I01.P01.S21.

Appendix A. Supplementary data

Supplementary data to this article can be found online at https://doi.org/10.1016/j.ijhydene.2024.05.028.

References

[1] Nemmour A, Inayat A, Janajreh I, Ghenai C. Green hydrogen-based E-fuels (E-methane, E-methanol, E-ammonia) to support clean energy transition: a literature review. Int J Hydrogen Energy 2023;48:29011–33. https://doi.org/10.1016/j.ijhydene.2023.03.240.

[2] Topolski K, Reznicek EP, Burcin CE, San Marchi CW, Ronevich JA, Fring L, Simmons K, Guerra Fernandez OJ, Hodge BM, Chung M. Hydrogen blending into natural gas pipeline infrastructure: review of the state of technology. Natl Renew Energy Lab, Golden CO; 2022. NREL/TP5400-81704.

[3] Bard J, Gerhardt N, Selzam P, Beil M, Wiemer M, Buddensiek M. The limitations of hydrogen blending in the European gas grid. Fraunhofer Inst Energy Econ Energy Syst Technol (IEE), Kassel; 2022.

[4] Quarton CJ, Samsatli S. Power-to-gas for injection into the gas grid: what can we learn from real-life projects, economic assessments and systems modelling? Renew Sustain Energy Rev 2018;98:302–16. https://doi.org/10.1016/j.rser.2018.09.007.

[5] Erdener BC, Sergi B, Guerra OJ, Chueca AL, Pambour K, Brancucci C, Hodge B-M. A review of technical and regulatory limits for hydrogen blending in natural gas pipelines. Int J Hydrogen Energy 2023;48:5595–617. https://doi.org/10.1016/j.ijhydene.2022.10.254.

[6] Lo Basso G, Pastore LM, Sgaramella A, Mojtahed A, de Santoli L. Recent progresses in H_2NG blends use downstream Power-to-Gas policies application: an overview over the last decade. Int J Hydrogen Energy 2024;51:424–453. https://doi.org/10.1016/j.ijhydene.2023.06.141.

[7] Makaryan IA, Sedov IV, Salgansky EA, Arutyunov AV, Arutyunov VS. A comprehensive review on the prospects of using hydrogen–methane blends: challenges and opportunities. Energies 2022;15:2265. https://doi.org/10.3390/en15062265.

[8] Rodrigues NS, McDonald CT, Busari OO, Satija A, Lucht RP. Transverse injection of rich, premixed, natural gas-air and natural gas-hydrogen-air reacting jets into high-speed vitiated crossflow at engine-relevant conditions. Int J Hydrogen Energy 2021;46:35718–38. https://doi.org/10.1016/j.ijhydene.2021.08.108.

[9] Fichtner J, Gegner A, Ninow J, Kapischke J. Hydrogen enriched natural gas as fuel for CHP units. Int J Hydrogen Energy 2023;48:35280–90. https://doi.org/10.1016/j.ijhydene.2023.05.263.

[10] Schwarz S, Daurer G, Gaber C, Demuth M, Prieler R, Hochenauer C. Experimental investigation of the combustion characteristics in oxy-fuel combustion of hydrogen-enriched natural gas on a semi-industrial scale. Int J Hydrogen Energy 2024,;49:323–37. https://doi.org/10.1016/j.ijhydene., 2023.07.268.

[11] Jia G, Lei M, Li M, Xu W, Li R, Lu Y, Cai M. Hydrogen embrittlement in hydrogen-blended natural gas transportation systems: a review. Int J Hydrogen Energy 2023;48:32137–57. https://doi.org/10.1016/j.ijhydene.2023.04.266.

[12] Wu X, Zhang H, Yang M, Jia W, Qiu Y, Lan L. From the perspective of new technology of blending hydrogen into natural gas pipelines transmission: mechanism, experimental study, and suggestions for further work of hydrogen embrittlement in high-strength pipeline steels. Int J Hydrogen Energy 2022;47:8071–90. https://doi.org/10.1016/j.ijhydene.2021.12.108.

[13] Wang H, Tong Z, Zhou G, Zhang C, Zhou H, Wang Y, Zheng W. Research and demonstration on hydrogen compatibility of pipelines: a review of current status and challenges. Int J Hydrogen Energy 2022;47:28585–604. https://doi.org/10.1016/j.ijhydene.2022.06.158.

[14] Kontogeorgis GM, Dohrn R, Economou IG, de Hemptinne J-C, ten Kate A, Kuitunen S, Mooijer M, Fele Žilnik L, Vesovic V. Industrial requirements for thermodynamic and transport properties: 2020. Ind Eng Chem Res 2021;60:4987–5013. https://doi.org/10.1021/acs.iecr.0c05356.

[15] Hendriks E, Kontogeorgis GM, Dohrn R, de Hemptinne JC, Economou IG, Fele Žilnik L. Vesovic V. Industrial requirements for thermodynamics and transport properties. Ind Eng Chem Res 2010;49:11131–41. https://doi.org/10.1021/ie101231b.

[16] Farzaneh-Gord M, Baghestani M, Rahbari HR. Prediction of natural gas density using only three measurable properties: intelligence and mathematical approaches. Energy Sources, Part A Recover Util Environ Eff 2022;44:393–412. https://doi.org/10.1080/15567036.2022.2045391.

[17] Farzaneh-Gord M, Rahbari HR. Numerical procedures for natural gas accurate thermodynamic properties calculation. J Eng Thermophys 2012;21:213–34. https://doi.org/10.1134/S1810232812040017.

[18] Farzaneh-Gord M, Rahbari HR, Mohseni-Gharesafa B, Toikka A, Zvereva I. Accurate determination of natural gas compressibility factor by measuring temperature, pressure and Joule-Thomson coefficient: artificial neural network approach. J Pet Sci Eng 2021;202:108427. https://doi.org/10.1016/j.petrol.2021.108427.

[19] Transmission Measurement Committee. AGA Report No. 8 Part 1. Thermodynamic properties of natural gas and related gases. DETAIL and GROSS equations of state. Third Ed. Washington DC: American Gas Association; 2017.

[20] Kunz O, Klimeck R, Wagner W, Jaeschke M. GERG Technical Monograph 15. The GERG-2004 wide-range equation of state for natural gases and other mixtures. Düsseldorf: Fortschritt-Berichte VDI; 2007.

[21] Kunz O, Wagner W. The GERG-2008 wide-range equation of state for natural gases and other mixtures: an expansion of GERG-2004. J Chem Eng Data 2012;57:3032–91. https://doi.org/10.1021/je300655b.

[22] Lozano-Martín D, Moreau A, Chamorro CR. Thermophysical properties of hydrogen mixtures relevant for the development of the hydrogen economy: review of available experimental data and thermodynamic models. Renew Energy 2022;198:1398–429. https://doi.org/10.1016/j.renene.2022.08.096.

[23] Deymi-Dashtebayaz M, Ebrahimi-Moghadam A, Pishbin SI, Pourramezan M. Investigating the effect of hydrogen injection on natural gas thermo-physical properties with various compositions. Energy 2019;167:235–45. https://doi.org/10.1016/j.energy.2018.10.186.

[24] Al Ghafri SZS, Jiao F, Hughes TJ, Arami-Niya A, Yang X, Siahvashi A, Karimi A, May EF. Natural gas density measurements and the impact of accuracy on process design. Fuel 2021;304:121395. https://doi.org/10.1016/j.fuel.2021.121395.

[25] International Organization for Standardization. ISO 6142-1 Gas analysis — preparation of calibration gas mixtures — Part 1: gravimetric method for Class I mixtures. 2014. Genève.

[26] International Organization for Standardization. ISO 12963. Gas analysis – comparison methods for the determination of the composition of gas mixtures based on one- and two-point calibration. 2017. Genève.

[27] Hernández-Gómez R, Tuma D, Lozano-Martín D, Chamorro CR. Accurate experimental (p, ρ, T) data of natural gas mixtures for the assessment of reference equations of state when dealing with hydrogen-enriched natural gas. Int J Hydrogen Energy 2018;43:21983–98. https://doi.org/10.1016/j.ijhydene.2018.10.027.

[28] Joint Commitee for Guides in Metrology. Evaluation of measurement data — Guide to the expression of uncertainty in measurement,. JCGM 100:2008 GUM 1995 with minor corrections 2008.
[29] Lemmon EW, Bell IH, Huber ML, McLinden MO. NIST standard reference database 23: reference fluid thermodynamic and transport properties REFPROP. Gaithersburg MD: National Institute of Standands and Technology, Standard Reference Data Program; 2018. Release 10.0.
[30] Huber ML, Lemmon EW, Bell IH, McLinden MO. The NIST REFPROP database for highly accurate properties of industrially important fluids. Ind Eng Chem Res 2022; 61:15449–72. https://doi.org/10.1021/acs.iecr.2c01427.
[31] Kleinrahm R, Wagner W. Measurement and correlation of the equilibrium liquid and vapour densities and the vapour pressure along the coexistence curve of methane. J Chem Thermodyn 1986;18:739–60. https://doi.org/10.1016/0021-9614(86)90108-4.
[32] Lösch HW, Kleinrahm R, Wagner W. Neue Magnetschwebewaagen für gravimetrische Messungen in der Verfahrenstechnik. Chem Ing Tech 1994;66: 1055–8. https://doi.org/10.1002/cite.330660808.
[33] Yang X, Kleinrahm R, McLinden MO, Richter M. The magnetic suspension balance: 40 Years of advancing densimetry and sorption science. Int J Thermophys 2023;44: 169. https://doi.org/10.1007/s10765-023-03269-0.
[34] Wagner W, Brachthäuser K, Kleinrahm R, Lösch HW. A new, accurate single-sinker densitometer for temperatures from 233 to 523 K at pressures up to 30 MPa. Int J Thermophys 1995;16:399–411. https://doi.org/10.1007/BF01441906.
[35] Klimeck J, Kleinrahm R, Wagner W. An accurate single-sinker densimeter and measurements of the (p, ρ, T) relation of argon and nitrogen in the temperature range from (235 to 520) K at pressures up to 30 MPa. J Chem Thermodyn 1998;30: 1571–88. https://doi.org/10.1006/jcht.1998.0421.
[36] McLinden MO, Kleinrahm R, Wagner W. Force transmission errors in magnetic suspension densimeters. Int J Thermophys 2007;28:429–48. https://doi.org/10.1007/s10765-007-0176-0.
[37] Lozano-Martín D, Mondéjar ME, Segovia JJ, Chamorro CR. Determination of the force transmission error in a single-sinker magnetic suspension densimeter due to the fluid-specific effect and its correction for use with gas mixtures containing oxygen. Measurement 2020;151:107176. https://doi.org/10.1016/j.measurement.2019.107176.
[38] Kleinrahm R, Yang X, McLinden MO, Richter M. Analysis of the systematic force-transmission error of the magnetic-suspension coupling in single-sinker densimeters and commercial gravimetric sorption analyzers. Adsorption 2019:25: 717–735. https://doi.org/10.1007/s10450-019-00071-z.
[39] Lozano-Martín D, Akubue GU, Moreau A, Tuma D, Chamorro CR. Accurate experimental (p, ρ, T) data of the ($CO_2 + O_2$) binary system for the development of models for CCS processes. J Chem Thermodyn 2020;150:106210. https://doi.org/10.1016/j.jct.2020.106210.
[40] Lozano-Martín D, Vega-Maza D, Martín MC, Tuma D, Chamorro CR. Thermodynamic characterization of the ($CO_2 + O_2$) binary system for the development of models for CCS processes: accurate experimental (p, ρ, T) data and virial coefficients. J Supercrit Fluids 2021;169:105074. https://doi.org/10.1016/j.supflu.2020.105074.
[41] Chamorro CR, Segovia JJ, Martín MC, Villamañán MA, Estela-Uribe JF, Trusler JPM. Measurement of the (pressure, density, temperature) relation of two (methane + nitrogen) gas mixtures at temperatures between 240 and 400 K and pressures up to 20 MPa using an accurate single-sinker densimeter. J Chem Thermodyn 2006;38:916–22. https://doi.org/10.1016/j.jct.2005.10.004.
[42] Mondéjar ME, Segovia JJ, Chamorro CR. Improvement of the measurement uncertainty of a high accuracy single sinker densimeter via setup modifications based on a state point uncertainty analysis. Measurement 2011;44:1768–80. https://doi.org/10.1016/j.measurement.2011.07.012.
[43] Taylor BN, Kuyatt CE, NIST Technical Note 1297. Guidelines for Evaluating and Expressing the Uncertainty of NIST Measurement Result. 1994.
[44] International Organization for Standardization. ISO 20765-2 Natural gas — calculation of thermodynamic properties — Part 2: single-phase properties (gas, liquid, and dense fluid) for extended ranges of application. 2013. Genève.
[45] Thol M, Richter M, May EF, Lemmon EW, Span R. EOS-LNG: a fundamental equation of state for the calculation of thermodynamic properties of liquefied natural gases. J Phys Chem Ref Data 2019;48:033102. https://doi.org/10.1063/1.5093800.
[46] Beckmüller R, Thol M, Bell IH, Lemmon EW, Span R. New equations of state for binary hydrogen mixtures containing methane, nitrogen, carbon monoxide, and carbon dioxide. J Phys Chem Ref Data 2021;50:013102. https://doi.org/10.1063/5.0040533.
[47] International Organization for Standardization. ISO 20765-1 Natural gas — calculation of thermodynamic properties — Part 1: gas phase properties for transmission and distribution applications. 2005. Genève.
[48] Lentner R, Richter M, Kleinrahm R, Span R. Density measurements of liquefied natural gas (LNG) over the temperature range from (105 to 135) K at pressures up to 8.9 MPa. J Chem Thermodyn 2017;112:68–76. https://doi.org/10.1016/j.jct.2017.04.002.
[49] Lentner R, Eckmann P, Kleinrahm R, Span R, Richter M. Density measurements of seven methane-rich binary mixtures over the temperature range from (100 to 180) K at pressures up to 9.7 MPa. J Chem Thermodyn 2020;142:106002. https://doi.org/10.1016/j.jct.2019.106002.
[50] Richter M, Ben Souissi MA, Span R, Schley P. Accurate (p, σ, T, x) measurements of hydrogen-enriched natural-gas mixtures at T = (273.15, 283.15, and 293.15) K with pressures up to 8 MPa. J Chem Eng Data 2014;59:2021–9. https://doi.org/10.1021/je500181v.
[51] Hernández-Gómez R, Tuma D, Pérez E, Chamorro CR. Accurate experimental (p, ρ, and T) data for the introduction of hydrogen into the natural gas grid (II): thermodynamic characterization of the methane-hydrogen binary system from 240 to 350 K and pressures up to 20 MPa. J Chem Eng Data 2018;63:1613–30. https://doi.org/10.1021/acs.jced.7b01125.
[52] Richter M, Kleinrahm R. Influence of adsorption and desorption on accurate density measurements of gas mixtures. J Chem Thermodyn 2014;74:58–66. https://doi.org/10.1016/j.jct.2014.03.020.
[53] Mondéjar ME, Fernández-Vicente TE, Haloua F, Chamorro CR. Experimental determination of (p, ρ, T) data for three mixtures of carbon dioxide with methane for the thermodynamic characterization of nonconventional energy gases. J Chem Eng Data 2012;57:2581–8. https://doi.org/10.1021/je300665n.